Comput Mech (2009) 43:321–340
DOI 10.1007/s00466-008-0308-9

ORIGINAL PAPER

Symmetric smoothed particle hydrodynamics (SSPH) method and its application to elastic problems

G. M. Zhang · R. C. Batra

Received: 4 February 2008 / Accepted: 4 June 2008 / Published online: 4 July 2008

Abstract We discuss the symmetric smoothed particle hydrodynamics (SSPH) method for generating basis functions for a meshless method. It admits a larger class of kernel functions than some other methods, including the smoothed particle hydrodynamics (SPH), the modified smoothed particle hydrodynamics (MSPH), the reproducing kernel particle method (RKPM), and the moving least squares (MLS) methods. For finding kernel estimates of derivatives of a function, the SSPH method does not use derivatives of the kernel function while other methods do, instead the SSPH method uses basis functions different from those employed to approximate the function. It is shown that the SSPH method and the RKPM give the same value of the kernel estimate of a function but give different values of kernel estimates of derivatives of the function. Results computed for a sine function defined on a one-dimensional domain reveal that the L^2, the H^1 and the H^2 error norms of the kernel estimates of a function computed with the SSPH method are less than those found with the MSPH method. Whereas the L^2 and the H^2 norms of the error in the estimates computed with the SSPH method are less than those with the RKPM, the H^1 norm of the error in the RKPM estimate is slightly less than that found with the SSPH method. The error norms for a sample problem computed with six kernel functions show that their rates of convergence with an increase in the number of uniformly distributed particles are the same and their magnitudes are determined by two coefficients related to the decay rate of the kernel function. The revised super Gauss function has the smallest error norm and is recommended as a kernel function in the SSPH method. We use the revised super Gauss kernel function to find the displacement field in a linear elastic rectangular plate with a circular hole at its centroid and subjected to tensile loads on two opposite edges. Results given by the SSPH and the MSPH methods agree very well with the analytic solution of the problem. However, results computed with the SSPH method have smaller error norms than those obtained from the MSPH method indicating that the former will give a better solution than the latter. The SSPH method is also applied to study wave propagation in a linear elastic bar.

Keywords Symmetric smoothed particle hydrodynamics (SSPH) method · Kernel function · Error norm · Meshless method

G. M. Zhang · R. C. Batra (✉)
Department of Engineering Science and Mechanics,
MC 0219, Virginia Polytechnic Institute and State University,
Blacksburg, VA 24061, USA
e-mail: rbatra@vt.edu

1 Introduction

The meshless Smoothed Particle Hydrodynamics (SPH) method, proposed by Lucy [1] to study three-dimensional (3D) astrophysics problems, has been successfully applied to find an approximate solution of many transient problems due to its simplicity and ease of applicability. However, it has two intrinsic shortcomings, namely, the lack of accuracy at boundary points, and the tensile instability. Many techniques, including the corrected smoothed particle method (CSPM) [2,3], the reproducing kernel particle method (RKPM) [4–6] and the modified smoothed particle hydrodynamics (MSPH) method [7,8] have been proposed to alleviate these two deficiencies. The performances of the CSPM and the MSPH methods for a sample problem have been compared in [7]; therefore, the CSPM is not further discussed here. Like the RKPM, the MSPH method can be made consistent of any desired order by retaining enough terms in the Taylor series expansion of the trial solution. However, the MSPH method

requires that all derivatives of the kernel function used in the method be non-constants which restrict the choice of the kernel function. Furthermore, the matrix to be inverted for finding kernel estimates of the unknown function and its derivatives is asymmetric. Here we study a Symmetric Smoothed Particle Hydrodynamics (SSPH) method that makes the matrix to be inverted symmetric, admits kernel functions with non-zero constant derivatives, and gives a better approximate solution than the MSPH method.

For a sine function defined on a 1D-domain, the L^2, the H^1 and the H^2 error norms of kernel estimates of the function have been computed with the SSPH, the MSPH and the RKP methods. It is found the L^2 and the H^2 error norms for the approximation obtained with the SSPH method are lower than those for the approximation derived with the RKPM, but the H^1 error norm for the approximation computed with the RKPM is less than that for the approximation with the SSPH method. The convergence rates of the error norms for the three methods with an increase in the number of either uniformly or non-uniformly spaced particles are nearly the same.

The kernel function plays an important role in meshless methods. Kernel functions generally used include spline [9] and Gauss functions [10]. Capuzzo-Dolcetta [11] has proposed a minimization procedure to select the kernel function in the SPH method; however, it becomes negative at some points within its compact support, which usually is not desirable. The effect of the kernel function on the accuracy of the computed solution has not been studied in detail. Here we compute results with six kernel functions, and propose a simple criterion to choose an appropriate kernel function. It is found that two constants related to the decay rate of a kernel function give good indication of the error in the kernel estimates of a function and its derivatives computed by using the kernel function.

The emphasis of the SSPH method proposed in [12] was to analyze numerically two plane stress/strain elasto-static problems by using either the collocation method or a weak formulation derived on a finite subregion of the given domain. It was found that basis functions with derivatives of the trial solution derived without differentiating basis functions for the trial solution gave a lower error than that in which derivatives of basis functions are used. Also, the numerical solution based on the weak formulation of the problem had a lower error than that based on the collocation method. The focus of the present work is to compare the SSPH basis functions with those derived by the MLS approximation and the RKPM, delineate the effect of six kernel functions on the accuracy of the numerical solution, and analyze an elasto-static and an elasto-dynamic problem.

We note that the concept of approximating a function and its derivatives by using different basis functions has been discussed in [13–18], and has also been adopted in the RKPM [19–22]. Interestingly, the final formulation of the SSPH method is similar to the reproducing kernel hierarchical partition of unity method and the synchronized reproducing kernel interpolant [15,16,23]. However, our approach of deriving basis functions is different from that employed in these works.

The rest of the paper is organized as follows. Section 2 describes briefly the MSPH method, and Sect. 3 gives details of the SSPH method. In Sect. 4, the RKPM is described for a 1D problem, and kernel estimates of a function and its derivatives computed with the RKPM and the SSPH method are compared with each other. The moving least squares (MLS) basis functions are compared with the SSPH basis functions in Sect. 5. Several numerical tests are performed in Sect. 6.1 to compare the accuracy of results computed with the RKPM, the SSPH method, and the MSPH method. Results obtained with the SSPH method using different kernel functions are compared in Sect. 6.2 to exhibit that two constants determined from values of the kernel function at three adjacent particles control the accuracy of the computed solution. Modifications for optimizing the performance of the super Gauss function are proposed. The SSPH method with the super Gauss kernel function is employed in Sect. 6.3 to solve a 2D linear elastostatic problem of a rectangular plate with a circular hole at its centroid and pulled at two opposite edges. Results computed with the SSPH basis functions are found to have smaller values of error norms than those obtained with the MSPH basis functions. A linear elastodynamic problem, namely wave propagation in a bar, is solved with the SSPH basis functions in Sect. 6.4. Conclusions of this work are summarized in Sect. 7.

2 Modified smoothed particle hydrodynamics (MSPH) method

The Taylor series expansion of a scalar function $f(\mathbf{x})$ at the point $\mathbf{x} = \mathbf{x}^{(i)}$ in a 3D-domain is

$$f(\boldsymbol{\xi}) = f(\mathbf{x}^{(i)}) + \frac{\partial f}{\partial x_\alpha^{(i)}}\left(\xi_\alpha - x_\alpha^{(i)}\right) + \frac{1}{2}\frac{\partial^2 f}{\partial x_\alpha^{(i)} \partial x_\beta^{(i)}}\left(\xi_\alpha - x_\alpha^{(i)}\right)\left(\xi_\beta - x_\beta^{(i)}\right) + \cdots \tag{2.1}$$

where repeated indices α and β are summed over their ranges, but the repeated index i enclosed in parentheses is not summed. We introduce two matrices, $\mathbf{P}$ and $\mathbf{Q}$, and rewrite Eq. (2.1) as

$$f(\boldsymbol{\xi}) = \mathbf{PQ} + \cdots \tag{2.2}$$

where

$$\mathbf{Q} = \Big\{ f_i, f_{x_1 i}, f_{x_2 i}, f_{x_3 i}, \frac{1}{2} f_{x_1 x_1 i}, \frac{1}{2} f_{x_2 x_2 i}, \frac{1}{2} f_{x_3 x_3 i}, f_{x_1 x_2 i}, f_{x_2 x_3 i}, f_{x_3 x_1 i} \Big\}^T, \tag{2.3}$$

$$\mathbf{P} = \Big\{ 1, \xi_1 - x_1^{(i)}, \xi_2 - x_2^{(i)}, \xi_3 - x_3^{(i)}, \left(\xi_1 - x_1^{(i)}\right)^2, \left(\xi_2 - x_2^{(i)}\right)^2, \left(\xi_3 - x_3^{(i)}\right)^2, \left(\xi_1 - x_1^{(i)}\right)\left(\xi_2 - x_2^{(i)}\right), \left(\xi_2 - x_2^{(i)}\right)\left(\xi_3 - x_3^{(i)}\right), \left(\xi_3 - x_3^{(i)}\right)\left(\xi_1 - x_1^{(i)}\right) \Big\}, \tag{2.4}$$

$$f_i = f(\mathbf{x}^{(i)}), \quad f_{x_\alpha i} = \frac{\partial f}{\partial x_\alpha}(x^{(i)}), \quad f_{x_\alpha x_\beta i} = \frac{\partial^2 f}{\partial x_\alpha \partial x_\beta}(\mathbf{x}^{(i)}). \tag{2.5}$$

Elements of matrix $\mathbf{Q}$ are the unknown variables to be found. As should become clear from the discussion given in Sect. 3, elements of matrix $\mathbf{P}$ can be associated with shape functions used in the Finite Element Method (FEM).

Multiplying both sides of Eq. (2.2) with a kernel function $W_i(\boldsymbol{\xi}, h) \equiv W(\mathbf{x}^{(i)} - \boldsymbol{\xi}, h)$, integrating the resulting equation over the domain Ω, and neglecting third and higher order derivative terms, we get

$$\int_\Omega f(\boldsymbol{\xi}) W_i d\boldsymbol{\xi} \approx \int_\Omega \mathbf{P}\mathbf{Q} W_i d\boldsymbol{\xi}. \tag{2.6}$$

In Eq. (2.6), the matrix $\mathbf{P}$ is known, but the number of unknowns in matrix $\mathbf{Q}$ exceeds the number of equations, which is one. Thus, additional equations are needed to solve for the unknown elements of matrix $\mathbf{Q}$. Multiplying both sides of Eq. (2.2) with kernel function's first derivative $W_{\xi_\gamma} = \partial W/\partial \xi_\gamma$, and its second derivative $W_{\xi_\gamma \xi_\delta} = \partial^2 W/\partial \xi_\gamma \partial \xi_\delta$ evaluated at the point $\mathbf{x}^{(i)}$ and integrating the resulting equations over the domain Ω, we obtain

$$\int_\Omega f(\boldsymbol{\xi}) W_{\xi_\gamma} d\boldsymbol{\xi} \approx \int_\Omega \mathbf{P}\mathbf{Q} W_{\xi_\gamma} d\boldsymbol{\xi}, \tag{2.7}$$

$$\int_\Omega f(\boldsymbol{\xi}) W_{\xi_\gamma \xi_\delta} d\boldsymbol{\xi} \approx \int_\Omega \mathbf{P}\mathbf{Q} W_{\xi_\gamma \xi_\delta} d\boldsymbol{\xi}. \tag{2.8}$$

Equations (2.6)–(2.8) can simultaneously be solved for the unknown element of matrix $\mathbf{Q}$. In terms of the matrix $\mathbf{M}$ defined as

$$\mathbf{M} = \Big\{ W, W_{\xi_1}, W_{\xi_2}, W_{\xi_3}, W_{\xi_1 \xi_1}, W_{\xi_2 \xi_2}, W_{\xi_3 \xi_3}, W_{\xi_1 \xi_2}, W_{\xi_2 \xi_3}, W_{\xi_1 \xi_3} \Big\}^T, \tag{2.9}$$

Eqs. (2.6)–(2.8) can be written as

$$\mathbf{T} = \mathbf{K}\mathbf{Q} \text{ or } T_I = K_{IJ} Q_J, \tag{2.10}$$

where

$$T_I = \int_\Omega f(\boldsymbol{\xi}) M_I d\boldsymbol{\xi}, \quad K_{IJ} = \int_\Omega M_I P_J d\boldsymbol{\xi}. \tag{2.11}$$

A suitable number, N_{total}, of particles are appropriately located in the domain Ω, and domain integrals in Eq. (2.11) are approximated by

$$\begin{aligned} T_I &= \int_\Omega f(\xi) M_I d\xi \approx \sum_{j=1}^{N^{(i)}} f_j M_I^{(j)} \frac{m_j}{\rho_j}, \\ K_{IJ} &= \int_\Omega M_I P_J d\xi \approx \sum_{j=1}^{N^{(i)}} M_I^{(j)} P_J^{(j)} \frac{m_j}{\rho_j} \end{aligned} \tag{2.12}$$

where $f_j = f(\boldsymbol{\xi}^{(j)})$, and $M_I^{(j)}$ is the value of M_I at $\boldsymbol{\xi}^{(j)}$. For particle i, located at the place $\mathbf{x}^{(i)}$, the mass m_i, and the mass density ρ_i are computed from the given data; the number $N^{(i)}$ of particles (or nodes) appearing in Eq. (2.12) is smaller than N_{total}, and represents particles that are in the compact support of the kernel function for particle i. It is clear that the matrix $\mathbf{K}$ defined by Eq. $(2.12)_2$ is not symmetric. In Eq. (2.12) one can replace m_i/ρ_i by the volume of domain Ω associated with the particle i.

We first find conditions for the matrix $\mathbf{K}$ to be non-singular. We note that for particle i, the matrix $\mathbf{K}$ can be written as

$$\begin{aligned} \mathbf{K} &= \begin{bmatrix} \sum_{j=1}^{N^{(i)}} M_1^{(j)} P_1^{(j)} \frac{m_j}{\rho_j} & \sum_{j=1}^{N^{(i)}} M_1^{(j)} P_2^{(j)} \frac{m_j}{\rho_j} & \cdots & \sum_{j=1}^{N^{(i)}} M_1^{(j)} P_{10}^{(j)} \frac{m_j}{\rho_j} \\ \sum_{j=1}^{N^{(i)}} M_2^{(j)} P_1^{(j)} \frac{m_j}{\rho_j} & \sum_{j=1}^{N^{(i)}} M_2^{(j)} P_2^{(j)} \frac{m_j}{\rho_j} & \cdots & \sum_{j=1}^{N^{(i)}} M_2^{(j)} P_{10}^{(j)} \frac{m_j}{\rho_j} \\ \vdots & \vdots & \ddots & \vdots \\ \sum_{j=1}^{N^{(i)}} M_{10}^{(j)} P_1^{(j)} \frac{m_j}{\rho_j} & \sum_{j=1}^{N^{(i)}} M_{10}^{(j)} P_2^{(j)} \frac{m_j}{\rho_j} & \cdots & \sum_{j=1}^{N^{(i)}} M_{10}^{(j)} P_{10}^{(j)} \frac{m_j}{\rho_j} \end{bmatrix} \\ &= \begin{bmatrix} M_1^{(1)} \frac{m_1}{\rho_1} & M_1^{(2)} \frac{m_2}{\rho_2} & \cdots & M_1^{(N^{(i)})} \frac{m_{N^{(i)}}}{\rho_{N^{(i)}}} \\ M_2^{(1)} \frac{m_1}{\rho_1} & M_2^{(2)} \frac{m_2}{\rho_2} & \cdots & M_2^{(N^{(i)})} \frac{m_{N^{(i)}}}{\rho_{N^{(i)}}} \\ \vdots & \vdots & \ddots & \vdots \\ M_{10}^{(1)} \frac{m_1}{\rho_1} & M_{10}^{(2)} \frac{m_2}{\rho_2} & \cdots & M_{10}^{(N^{(i)})} \frac{m_{N^{(i)}}}{\rho_{N^{(i)}}} \end{bmatrix} \\ &\quad \times \begin{bmatrix} P_1^{(1)} & P_2^{(1)} & \cdots & P_{10}^{(1)} \\ P_1^{(2)} & P_2^{(2)} & \cdots & P_{10}^{(2)} \\ \vdots & \vdots & \ddots & \vdots \\ P_1^{(N^{(i)})} & P_2^{(N^{(i)})} & \cdots & P_{10}^{(N^{(i)})} \end{bmatrix} \end{aligned} \tag{2.13}$$

where matrix $\mathbf{K}$ equals the product of a $10 \times N^{(i)}$ matrix and a $N^{(i)} \times 10$ matrix. By the Binet–Cauchy Theorem [24], the

determinant of matrix **K** is given by

$$Det\,[\mathbf{K}] = \sum_{\substack{N_1,N_2,\ldots,N_{10}=1\\ N_1<N_2<\cdots N_9<N_{10}}}^{N^{(i)}} \left\{ \prod_{k=N_1,N_2,\ldots,N_{10}} \left[\frac{m_k}{\rho_k}\right] Det \begin{bmatrix} M_1^{(N_1)} & M_1^{(N_2)} & \cdots & M_1^{(N_{10})} \\ M_2^{(N_1)} & M_2^{(N_2)} & \cdots & M_2^{(N_{10})} \\ \vdots & \vdots & \ddots & \vdots \\ M_{10}^{(N_1)} & M_{10}^{(N_2)} & \cdots & M_{10}^{(N_{10})} \end{bmatrix} \times Det \begin{bmatrix} P_1^{(N_1)} & P_2^{(N_1)} & \cdots & P_{10}^{(N_1)} \\ P_1^{(N_2)} & P_2^{(N_2)} & \cdots & P_{10}^{(N_2)} \\ \vdots & \vdots & \ddots & \vdots \\ P_1^{(N_{10})} & P_2^{(N_{10})} & \cdots & P_{10}^{(N_{10})} \end{bmatrix} \right\} \tag{2.14}$$

Here $N_1, N_2, \ldots, N_{10}$ are any ten particles in the ascending order from 1 to $N^{(i)}$, and $P_I^{(N_1)}$, $M_I^{(N_1)}$ denote values of P_I and M_I at the particle N_1. Because polynomial functions in Eq. (2.4) are linearly independent, and the matrix **M** is non-singular since det [**M**] equals the Wronskian of the function W, the determinant of matrix **K** is not zero. Thus the necessary condition for the matrix **K** to be non-singular is that the number of particles in the compact support of the kernel function for a particle equal at least the number of linearly independent monomials in Eq. (2.4). Furthermore, all derivatives of the kernel function appearing in matrix **M** must not be constants. This latter requirement restricts the choice of the kernel function.

Equation (2.10) can be written as

$$\mathbf{Q} = \mathbf{K}^{-1}\mathbf{T}. \tag{2.15}$$

For the MSPH method, the kernel estimates of a function, and its first, and second order derivatives are consistent up to orders m, $(m-1)$ and $(m-2)$, respectively, if up to m order terms are retained in the Taylor series expansion (2.1) of the function.

3 Symmetric smoothed particle hydrodynamics (SSPH) method

Rather than multiplying both sides of Eq. (2.2) by the kernel function and its derivatives, we multiply them with $W_i P_I$, neglect terms involving third and higher order derivatives, integrate the resulting equation over the domain Ω, and obtain

$$\int_\Omega f(\boldsymbol{\xi})\, W_i \mathrm{P_I} d\boldsymbol{\xi} \approx \int_\Omega \mathbf{PQ}\mathrm{P_I} W_i d\boldsymbol{\xi}. \tag{3.1}$$

We write Eq. (3.1) in matrix form as

$$\mathbf{T} = \mathbf{KQ} \text{ or } T_I = K_{IJ} Q_J, \tag{3.2}$$

where

$$T_I = \int_\Omega f(\xi) W_i P_I d\xi \approx \sum_{j=1}^{N^{(i)}} f_j W_{ij} P_I^{(j)} \frac{m_j}{\rho_j},$$
$$K_{IJ} = \int_\Omega P_I P_J W_i d\xi \approx \sum_{j=1}^{N^{(i)}} P_I^{(j)} P_J^{(j)} W_{ij} \frac{m_j}{\rho_j},$$
$$W_{ij} = W(x^{(i)} - \xi^{(j)}). \tag{3.3}$$

Thus the matrix **K** is symmetric which reduces storage requirements and the CPU time needed to solve Eq. (3.2) for **Q**. An interesting aspect of this alternative is that in Eq. (3.2) there are no derivatives of the kernel function. It allows for a much larger class of functions to be used as the kernel function, and hence improves the practicality and the usefulness of the method.

In order to show that the matrix **K** defined by Eq. (3.3) is non-singular, we follow a procedure similar to that used to show that the matrix **K** defined by Eq. (2.12) is non-singular. Indeed, we replace M_I with $W_i P_I$ in Eq. (2.14) and obtain the following for the determinant of matrix **K**:

$$Det[\mathbf{K}] = \sum_{\substack{N_1,N_2,\ldots,N_{10}=1\\ N_1<N_2<\cdots N_9<N_{10}}}^{N^{(i)}} \left\{ \prod_{k=N_1,N_2,\ldots,N_{10}} \left(W_{ik}\frac{m_k}{\rho_k}\right) \times Det \begin{bmatrix} P_1^{(N_1)} & P_2^{(N_1)} & \cdots & P_{10}^{(N_1)} \\ P_1^{(N_2)} & P_2^{(N_2)} & \cdots & P_{10}^{(N_2)} \\ \vdots & \vdots & \ddots & \vdots \\ P_1^{(N_{10})} & P_2^{(N_{10})} & \cdots & P_{10}^{(N_{10})} \end{bmatrix}^2 \right\}. \tag{3.4}$$

Here $N_1, N_2, \ldots, N_{10}$ are any ten particles in the ascending order from 1 to $N^{(i)}$. For reasons stated in Sect. 2, the determinant of matrix **K** is non-zero.

For a 1D problem, $P = \left\{1, \xi - x^{(i)}, \left(\xi - x^{(i)}\right)^2\right\}$, $P_2 = \left(\xi - x^{(i)}\right)$. Using Vandermonde's rule [25], Eq. (3.4) reduces to

$$Det[\mathbf{K}] = \sum_{\substack{N_1,\,N_2,\,N_3=1\\ N_1<N_2<N_3}}^{N^{(i)}} \left\{ \prod_{k=N_1,N_2,N_3} \left(W_{ik}\frac{m_k}{\rho_k}\right) \times \left[\left(P_2^{(N_2)}-P_2^{(N_1)}\right)\left(P_2^{(N_3)}-P_2^{(N_2)}\right) \times \left(P_2^{(N_3)}-P_2^{(N_1)}\right)\right]^2 \right\} \tag{3.5}$$

For $P_2^{(N_1)} \neq P_2^{(N_2)} \neq P_2^{(N_3)}$, the determinant will be different from zero. Thus for the matrix $\mathbf{K}$ to be nonsingular, the necessary and sufficient condition is that the compact support of a particle's kernel include at least two other particles (having different coordinates).

Since the matrix $\mathbf{K}$ is symmetric, we designate this method as symmetric smoothed particle hydrodynamics (SSPH) method.

Equation (3.2) has the solution

$$\mathbf{Q} = \mathbf{K}^{-1}\mathbf{T}. \tag{3.6}$$

The matrix $\mathbf{K}^{-1}$ is symmetric. For a 1D-problem Eq. (3.6) can be written as

$$\begin{aligned} f_i &= \int_\Omega \mathbf{PK}^{-1}\{1,0,0\}^T\, W\left(x^{(i)}-\xi\right) f(\xi)\, d\xi,\\ f_{xi} &= \int_\Omega \mathbf{PK}^{-1}\{0,1,0\}^T\, W\left(x^{(i)}-\xi\right) f(\xi)\, d\xi,\\ f_{xxi} &= \int_\Omega \mathbf{PK}^{-1}\{0,0,1\}^T\, W\left(x^{(i)}-\xi\right) f(\xi)\, d\xi. \end{aligned} \tag{3.7}$$

Or equivalently,

$$\begin{aligned} f_i &\approx \sum_{j=1}^{N^{(i)}} \mathbf{PK}^{-1}\{1,0,0\}^T\, W_{ij} f_j m_j/\rho_j,\\ f_{xi} &\approx \sum_{j=1}^{N^{(i)}} \mathbf{PK}^{-1}\{0,1,0\}^T\, W_{ij} f_j m_j/\rho_j,\\ f_{xxi} &\approx \sum_{j=1}^{N^{(i)}} \mathbf{PK}^{-1}\{0,0,1\}^T\, W_{ij} f_j m_j/\rho_j. \end{aligned} \tag{3.8}$$

We rewrite Eq. (3.8) as

$$f_i^{(k)} \approx \sum_{j=1}^{N^{(i)}} N_{ij}(k)\, f_j,\ k=0,1,2, \tag{3.9}$$

where $f_i^{(k)}$ equals the kth derivative of f evaluated at the point $x^{(i)}$, and

$$\begin{aligned} N_{ij}(1) &= PK^{-1}\{1,0,0\}^T\, W_{ij} m_j/\rho_j,\\ N_{ij}(2) &= PK^{-1}\{0,1,0\}^T\, W_{ij} m_j/\rho_j,\\ N_{ij}(3) &= PK^{-1}\{0,0,1\}^T\, W_{ij} m_j/\rho_j. \end{aligned} \tag{3.10}$$

Note that indices i and j in Eq. (3.10) are not tensorial indices. The function $N_{ij}(k)$ can be viewed as a shape function for the node located at $x^{(i)}$. That is, shape functions for f, its first derivative f_x, and its second derivative f_{xx} at particle $x^{(i)}$ are different. Recall that in the FEM,

$$f_i^{(k)} = \sum_{j=1}^{N} \frac{d^k}{dx^k}\left(N_j\right) f_j, \quad k=0,1,2,\ldots. \tag{3.11}$$

For $k=0$, the kernel estimate (3.9) of the function in the SSPH method is exactly of the same form as that in the FEM. However, for $k \neq 0$, expressions for kernel estimates of the first and the second derivatives are different from those in the FEM. In order to compute kernel estimates of derivatives in the SSPH method, we do not differentiate the shape functions. Instead we use another set of shape functions.

As for the MSPH method, the kernel estimates of a function, and of its first and second derivatives are consistent of order m, $(m-1)$ and $(m-2)$, respectively, when terms up to order m are retained in the Taylor series expansion (2.1) of the function.

The basis functions (3.10) have been derived without using any connectivity among particles. Therefore, like the MLS basis functions [26], these can be used as basis to solve an initial-boundary-value problem. We note that like the MLS basis functions the SSPH basis functions (3.10) do not exhibit the Kronecker delta property.

4 Comparison of the SSPH method with the RKPM

The RKPM [4–6] improves the traditional SPH method, and is briefly described below for a 1D problem. The kernel estimate of a function $f(x)$ in the SPH method is given by

$$f(x) \approx \int_\Omega f(\xi)\, W(x-\xi)\, d\xi. \tag{4.1}$$

The traditional SPH method proposed by Lucy [1] does not have zeroth-order consistency at the boundaries. In the RKPM it is remedied by modifying the kernel function to $\overline{W}(x-\xi)$ defined by

$$\overline{W}(x-\xi) = W(x-\xi)\, C(x-\xi), \tag{4.2}$$

where $C(x-\xi)$ is a correction to the kernel function. Expanding the function $f(\xi)$ in terms of Taylor series around

the point x, and setting

$$\tilde{m}_k(x) = \int_\Omega (x-\xi)^k \overline{W}(x-\xi)\, d\xi \quad k = 0, 1, 2, \ldots, n, \tag{4.3}$$

Eq. (4.1) can be written as

$$f(x) = \tilde{m}_0(x) f(x) - \tilde{m}_1(x) f'(x) + \cdots + \frac{(-1)^n}{n!}\tilde{m}_n f^{(n)}(x) + \cdots . \tag{4.4}$$

In order to reproduce the original function, the correction kernel is chosen by setting coefficients of the first and the higher order derivatives to zero and the coefficient of the constant term to one. That is,

$$\frac{(-1)^n}{n!}\tilde{m}_n(x) = \delta_{n0}, \tag{4.5}$$

where δ_{ij} is the Kronecker delta. Generally $C(x-\xi)$ in the corrected kernel (4.2) is chosen to be the polynomial function

$$\mathbf{C}(x-\xi) \approx \mathbf{Pb}, \tag{4.6}$$

where the matrix $\mathbf{P}$ is given by Eq. (2.4), and $\mathbf{b} = [b_0(x), b_1(x), \ldots, b_n(x)]^T$. The k^{th} order moment of the corrected kernel function can be written as

$$\begin{aligned}\tilde{m}_k(x) &= \int_\Omega (x-\xi)^k C(x-\xi) W d\xi \\ &= \int_\Omega (x-\xi)^k \mathbf{Pb} W(x-\xi)\, d\xi \\ &= b_0(x) m_k(x) + b_1(x) m_{k+1}(x) + \cdots \\ &\quad + b_n(x) m_{k+n}(x)\end{aligned} \tag{4.7}$$

where $m_k(x)$ is the k^{th} order moment of the original kernel $W(x-\xi)$.

From Eqs. (4.5) and (4.7), we get

$$\mathbf{M}(x)\mathbf{b}(x) = \{1, 0, 0\}^T = \mathbf{P}^T(0), \tag{4.8}$$

where

$$\mathbf{M}(x) = \begin{bmatrix} m_0(x) & m_1(x) & \cdots & m_n(x) \\ m_1(x) & m_2(x) & \cdots & m_{n+1}(x) \\ \vdots & \vdots & \ddots & \vdots \\ m_n(x) & m_{n+1}(x) & \cdots & m_{2n}(x) \end{bmatrix}. \tag{4.9}$$

We note that the matrix $\mathbf{M}$ is the same as the matrix $\mathbf{K}$ defined in the SSPH method. We use below the matrix $\mathbf{K}$ instead of the matrix $\mathbf{M}$ and write Eq. (4.8) as

$$\mathbf{b}(x) = \mathbf{K}^{-1}(x)\mathbf{P}^T(0). \tag{4.10}$$

Substituting for $\mathbf{b}$ in Eq. (4.6) and the result in Eqs. (4.2) and (4.1), we get

$$f(x) = \int_\Omega \mathbf{Pb} W(x-\xi) f(\xi)\, d\xi. \tag{4.11}$$

Similarly, we obtain the following for the first and the second derivatives of the function $f(x)$:

$$\begin{aligned} f'(x) &= \int_\Omega f(\xi) \frac{d}{dx}\left[\mathbf{Pb} W(x-\xi)\right] d\xi, \\ f''(x) &= \int_\Omega f(\xi) \frac{d^2}{dx^2}\left[\mathbf{Pb} W(x-\xi)\right] d\xi, \end{aligned} \tag{4.12}$$

we note that

$$\begin{aligned} \mathbf{b}'(x) &= -\mathbf{K}^{-1}(x)\mathbf{K}'(x)\mathbf{b}(x), \\ \mathbf{b}''(x) &= -\mathbf{K}^{-1}(x)\left[\mathbf{K}''(x)\mathbf{b}(x) + 2\mathbf{K}'(x)\mathbf{b}'(x)\right], \end{aligned} \tag{4.13}$$

where $\mathbf{K}'(x)$ is the first derivative of the matrix $\mathbf{K}(x)$.

For the RKPM, we rewrite kernel estimates of the function $f(x)$ and of its first and second derivatives together in the matrix form as

$$\begin{Bmatrix} f_i \\ f_{xi} \\ f_{xxi} \end{Bmatrix} = \begin{Bmatrix} \int_\Omega \mathbf{Pb} W\left(x^{(i)}-\xi\right) f(\xi)\, d\xi \\ \int_\Omega \frac{d}{dx}\left[\mathbf{Pb} W\left(x^{(i)}-\xi\right)\right] f(\xi)\, d\xi \\ \int_\Omega \frac{d^2}{dx^2}\left[\mathbf{Pb} W\left(x^{(i)}-\xi\right)\right] f(\xi)\, d\xi \end{Bmatrix} \tag{4.14}$$

For the SSPH method, Eq. (3.7) gives

$$\begin{Bmatrix} f_i \\ f_{xi} \\ f_{xxi} \end{Bmatrix} = \begin{Bmatrix} \int_\Omega \mathbf{PK}^{-1}\{1,0,0\}^T W\left(x^{(i)}-\xi\right) f(\xi)\, d\xi \\ \int_\Omega \mathbf{PK}^{-1}\{0,1,0\}^T W\left(x^{(i)}-\xi\right) f(\xi)\, d\xi \\ \int_\Omega \mathbf{PK}^{-1}\{0,0,1\}^T W\left(x^{(i)}-\xi\right) f(\xi)\, d\xi \end{Bmatrix} \tag{4.15}$$

For $\mathbf{P}^T(0) = \{1, 0, 0\}^T$, expressions for kernel estimates of the function in Eqs. (4.14) and (4.15) are identical to each other. However, expressions for their first- and second-order derivatives are quite different. In the RKPM, the expression for the derivatives of $f(x)$ involves the derivative of the kernel function W through the derivative of the matrix $\mathbf{b}$. The requirement of using a differentiable kernel function restricts the choice of the kernel function as in the MSPH method. The evaluation of derivatives of the matrix $\mathbf{b}$ requires additional CPU time.

5 Comparison of the SSPH basis functions with the MLS basis functions

The MLS basis functions proposed by Lancaster and Salkauskas [26] have been widely used in meshless methods

[27,28]. The approximation of a function in the neighborhood of a point $\boldsymbol{x}$ is expressed as

$$f(\boldsymbol{x}) = \mathbf{P}(\boldsymbol{x})\,\mathbf{a}(\boldsymbol{x}), \tag{5.1}$$

where $\mathbf{a}$ is the coefficient matrix to be determined, and $\mathbf{P}$ is the matrix of complete monomials. The matrix $\mathbf{P} = \{1, x_1, x_2, x_3, x_1^2, \cdots\}$ is different from the matrix $\mathbf{P} = \{1, \xi_1 - x_1, \xi_2 - x_2, \xi_3 - x_3, (\xi_1 - x_1)^2, \ldots\}$ in the MSPH, the SSPH and the RKPMs. Eq. (5.1) can be transformed into the Taylor series expansion form of Eq. (2.1). For example, in 1D, and retaining two terms in the Taylor series expansion, we get

$$\begin{aligned} f_j &\approx f + f_x\left(x_j - x\right) + \frac{1}{2} f_{xx}\left(x_j - x\right)^2 \\ &\approx \left(f + f_x x_j + \frac{1}{2} f_{xx} x_j^2\right) - \left(f_x + f_{xx} x_j\right) x + \frac{1}{2} f_{xx} x^2 \end{aligned} \tag{5.2}$$

Thus the difference between Eqs. (2.1) and (5.1) is that the matrix $\mathbf{a}$ in the MLS basis functions has a different interpretation from the matrix $\mathbf{Q}$ in the SSPH basis functions. For a 1D-problem, $\mathbf{Q} = \{f, f_x, \frac{1}{2} f_{xx}\}$, and $\mathbf{a} = \{f + f_x x_j + \frac{1}{2} f_{xx} x_j^2, -f_x - f_{xx} x_j, \frac{1}{2} f_{xx}\}$. The coefficient matrix $\mathbf{a}$ is determined by minimizing the functional, J, that represents the weighted discrete L^2 error norm defined by

$$J = \sum_{j=1}^{N} W\left(x^{(j)} - \xi\right)\left(\mathbf{P}\left(x^{(j)}\right)\mathbf{a}(x) - f_j\right)^2, \tag{5.3}$$

where f_j is the fictitious value of the function at node or particle j and N equals the number of particles where the weight function or the kernel function W is non-zero. The minimization of J obtained by setting $\frac{\partial J}{\partial \mathbf{a}} = 0$ yields

$$\mathbf{A}\mathbf{a} = \mathbf{B}\mathbf{F}, \tag{5.4}$$

where $\mathbf{A} = \sum_{j=1}^{N} W_j \mathbf{P}^{(j)} \mathbf{P}^{(j)^T}$, $\mathbf{B} = [W_1 \mathbf{P}^{(1)^T}, W_2 \mathbf{P}^{(2)^T}, \ldots, W_N \mathbf{P}^{(N)^T}]$, $\mathbf{F} = [f_1, f_2, \ldots, f_N]^T$, $W_j = W(x^{(j)} - \xi)$ and $\mathbf{P}^{(N)} = \mathbf{P}\left(x^{(N)}\right)$.

With the definition $\mathbf{D} = \mathbf{B}\mathbf{F}$, we write Eq. (5.4) as

$$\mathbf{A}\mathbf{a} = \mathbf{D}, \quad A_{IJ} = \sum_{j=1}^{N} W_j P_I^{(j)} P_J^{(j)}, \quad D_I = \sum_{j=1}^{N} f_j W_j P_I^{(j)}, \tag{5.5}$$

where $P_I^{(j)}$ is the I^{th} element of matrix $\mathbf{P}$ evaluated at $\left(x^{(j)}\right)$. The comparison of Eqs. (5.5) and (3.2) reveals that except for the factor m_j/ρ_j and the matrix $\mathbf{P}$, matrices $\mathbf{A}$ and $\mathbf{K}$ are similar, and matrices $\mathbf{D}$ and $\mathbf{T}$ are similar. Thus matrices $\mathbf{a}$ and $\mathbf{Q}$ play similar roles as stated in the text following Eq. (5.2).

From Eq. (5.4), the coefficient matrix $\mathbf{a}$ can be determined as

$$\mathbf{a} = \mathbf{A}^{-1}\mathbf{B}\mathbf{F}. \tag{5.6}$$

Substituting for $\mathbf{a}$ from Eq. (5.6) into Eq. (5.1), the approximation of the function is given by

$$f(x) \approx \mathbf{P}\mathbf{A}^{-1}\mathbf{B}\mathbf{F} = \mathbf{\Phi}\mathbf{F} = \sum_{j=1}^{N} \Phi_j f_j, \tag{5.7}$$

where Φ may be regarded as the MLS basis function and f_j is the fictitious value of the function at particle j.

Derivatives of the function can be obtained by differentiating the shape functions in Eq. (5.7), i.e.,

$$f_x(x) \approx \mathbf{\Phi}_{,x}\mathbf{F} = \sum_{j=1}^{N} \Phi_{j,x} f_j. \tag{5.8}$$

Thus computation of f_x necessitates the differentiation of matrix $\mathbf{A}$ and hence of the kernel function which restricts choices of the kernel function. Whereas in the SSPH method, kernel estimates of the first and the second derivatives of a function are found by solving a system of linear algebraic equations, in the MLS approximation they are evaluated by differentiating the MLS basis functions like that in the FEM.

In order to evaluate derivatives of a function at a point, the kernel (or the weight) function needs to be differentiated when using the MSPH method, the RKPM, and the MLS approximation but not in the SSPH method.

6 Numerical examples

6.1 Comparison of approximations of a function with the RKPM, the MSPH method and the SSPH method

Consider the function

$$f(x) = \sin[8(1 - x)] / \sin 8 \tag{6.1}$$

defined on the domain [0,1]. We use the SSPH, the MSPH and the RKPM, to compute kernel estimates of the function and of its first and second derivatives with 10 equally spaced particles placed on the domain [0, 1]. The smoothing length, h, equals 1.5 times the minimum distance, $\Delta = 0.1$, between two adjacent particles.

We use the following revised Gauss function as the kernel function.

$$W(\mathbf{x} - \boldsymbol{\xi}) = \frac{G}{\left(h\sqrt{\pi}\right)^{\lambda}} \times \begin{cases} \left(e^{-(|\mathbf{x}-\boldsymbol{\xi}|^2/h^2)} - e^{-4}\right) & |\mathbf{x} - \boldsymbol{\xi}| \le 2h \\ 0 & |\mathbf{x} - \boldsymbol{\xi}| > 2h \end{cases} \tag{6.2}$$

Here λ equals the dimensionality of the space, and the normalization parameter G has values 1.04823, 1.10081, and 1.18516 for λ = 1, 2, and 3, respectively.

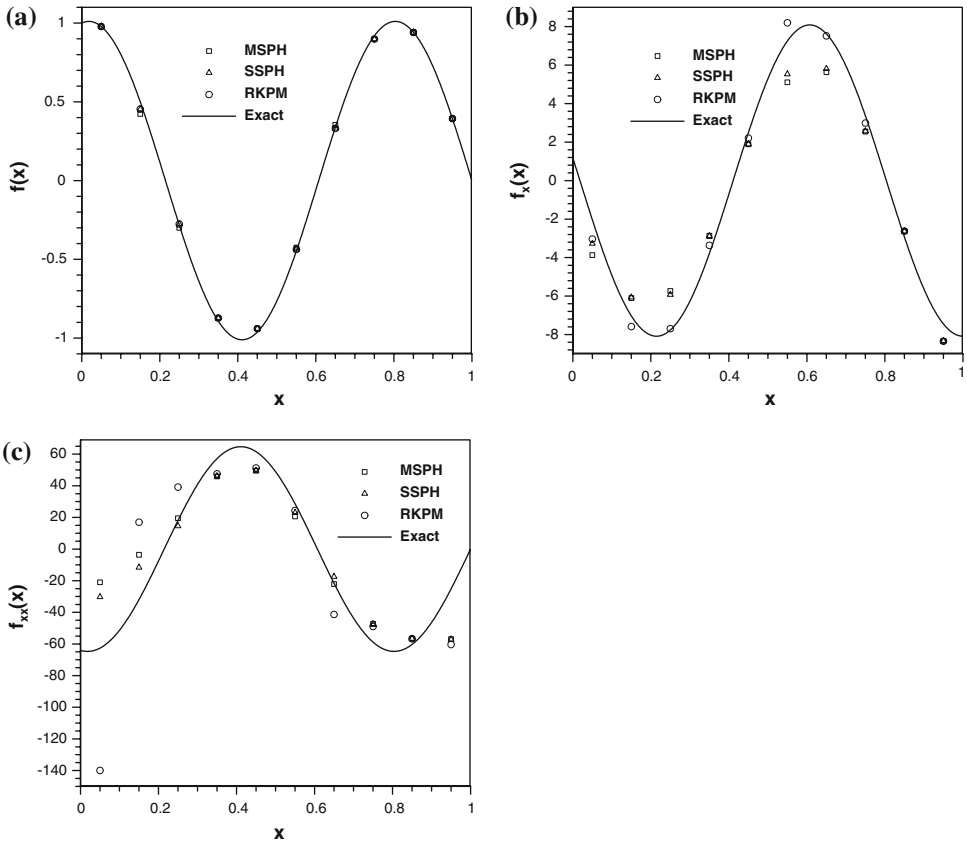

Fig. 1 Kernel estimates of (**a**) the function, its (**b**) first derivative, and (**c**) second derivative computed with the MSPH and the SSPH methods, and with the RKPM

We define below the L^2, the H^1 and the H^2 norms of the error, e, in the kernel estimates of the function f and of its first and second derivatives.

$$\|e\|_0 = \sqrt{\int_0^1 (f^{exact} - f^{compute})^2 \, dx}$$
$$\|e\|_1 = \sqrt{\int_0^1 \left(f_x^{exact} - f_x^{compute}\right)^2 dx} \tag{6.3}$$
$$\|e\|_2 = \sqrt{\int_0^1 \left(f_{xx}^{exact} - f_{xx}^{compute}\right)^2 dx}$$

Figure 1 shows kernel estimates of the function, and of its first and second derivatives computed with the three methods. It is obvious that each one of the three methods reconstructs the function very well with only ten particles distributed uniformly on [0,1]. In [7], it is shown that the error in kernel estimates of the function and its derivatives near the boundary is greatly reduced in the MSPH method as compared to that in the SPH method and the CSPM (corrective smoothed particle method). It is obvious from results depicted in Fig. 1 that kernel estimates of the function computed with the SSPH method and the RKPM are as accurate at the boundary as those found with the MSPH method. The SSPH method gives more accurate values of the first and the second derivatives of the function than the MSPH method. The first derivatives computed with the RKPM are better approximations of their analytical values than those computed either with the SSPH or with the MSPH method. However, values of the second derivatives computed with the RKPM near end points of the domain [0,1] are worse than those found with the SSPH and the MSPH methods.

The shape functions for the kernel estimate, the first and the second derivatives are shown in Fig. 2. It is seen from Fig. 2(a) that $\sum_j N_{ij}(1) = 1$, i.e., it is a partition of unity.

Values of the three error norms for approximations with the three methods listed in Table 1 reveal that all of the error norms for the SSPH basis functions are smaller than those for the MSPH basis functions. As shown above in Sect. 4, the RKPM and the SSPH method give identical values of kernel estimates of the function. The H^1 error norm is smallest for the RKPM, but its evaluation requires additional computational time. The H^2 error norm of the RKPM solution equals 32.8, which is 63.2 and 90.7% larger than that given by the MSPH and the SSPH basis functions, respectively.

Variations of the error norms with the particle distance, Δ, are exhibited in Fig. 3 on log-log plots for 10, 20, 30, 50, 100, 250 and 500 uniformly spaced particles. It is clear that irrespective of the number of particles, the L^2 error norm

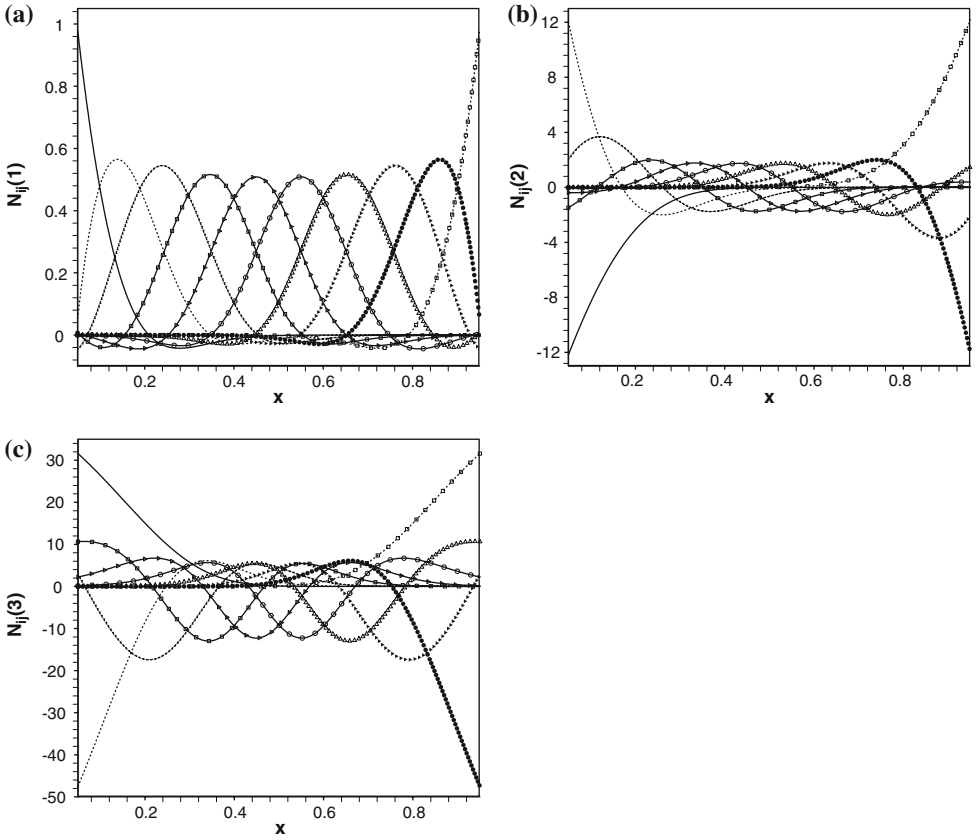

Fig. 2 For ten uniformly distributed particles on the domain [0,1], shape functions for (**a**) kernel estimate, (**b**) first derivative, and (**c**) second derivative

Table 1 Error norms for the RKPM, the MSPH and the SSPH methods

	MSPH	SSPH	RKPM
$\|\|e\|\|_0$	2.86E-2	1.88E-2	1.88E-2
$\|\|e\|\|_1$	1.40	1.21	0.59
$\|\|e\|\|_2$	20.1	17.2	32.8

Table 2 Convergence rates of error norms for the MSPH, the SSPH and the RKPM solutions

	MSPH	SSPH	RKPM
$\|e\|_0$	3.52	3.54	3.54
$\|e\|_1$	1.92	1.96	1.80
$\|e\|_2$	1.47	1.49	1.54

of the approximations with the SSPH and the RKPM basis functions are smaller than that of the MSPH basis functions. The RKPM gives the smallest value of the H^1 error norm and the largest value of the H^2 error norm. The convergence rates, i.e., slopes of the least squares fitted straight lines, for the three methods are listed in Table 2. For each one of the three methods, convergence rates of the L^2, the H^1 and the H^2 error norms equal approximately 3.5, 2.0 and 1.5, respectively. Larger differences in the convergence rates of the H^1 and the H^2 error norms between the RKPM and the MSPH/SSPH solutions are due to the noticeable deviations in the RKPM solution for values of x near $x = 0$ and $x = 1$.

Figure 4 shows results for the nonuniform particle distributions with the distance between particles $(i - 1)$ and i equaling $\Delta\ (i + 0.2(i - 1))$ where Δ equals the distance between particles 1 and 2 which is the smallest distance between any two adjacent particles. Results have been computed for 10, 20, 30, 50, 100, 250 and 500 particles. These results are similar to those obtained for the uniform particle distribution except that for small number of particles the H^2 error norm of the RKPM solution is less than that of the MSPH and the SSPH solutions. We did not experiment with other non-uniform distributions of particles.

6.2 Results for the SSPH method with different kernel functions

As noted earlier, the kernel function in the MSPH method must be such that none of its first and second order derivatives is a constant. Thus if we need kernel estimates of a function and of its m^{th} order derivatives then the order of the polynomial in the kernel function must be at least $(m + 1)$. However, there is no such restriction in the SSPH method.

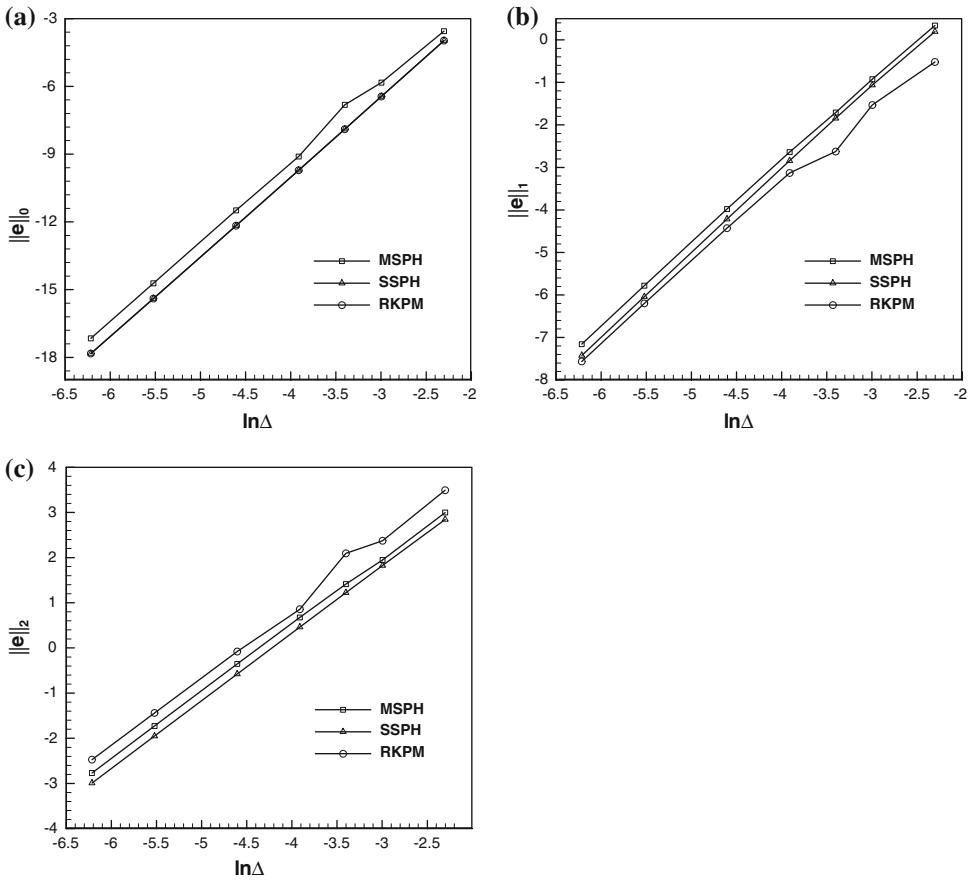

Fig. 3 Variation with different number of uniformly spaced particles of the (**a**) L^2 norm; (**b**) H^1 norm; and (**c**) H^2 norm of the error in kernel estimates of a function computed with the MSPH and the SSPH methods, and with the RKPM

We compare results with the following six kernel functions of which four, namely, the cubic spline [29], the quartic spline [30], the revised Gauss, and the super Gauss [31] functions, are often used in meshless methods, while the other two, namely the linear and the quadratic, cannot be used in some meshless methods including the SPH, the MSPH and the RKPMs if kernel estimates of the first and the second order derivatives are to be found.

Linear function:

$$W(d) = \frac{G}{h^{\lambda}} \begin{cases} (2-d)/4 & 0 \le d \le 2 \\ 0 & 2 < d \end{cases} \tag{6.4}$$

Quadratic function:

$$W(d) = \frac{G}{h^{\lambda}} \begin{cases} 1 - d + d^2/4 & 0 \le d \le 2 \\ 0 & 2 < d \end{cases} \tag{6.5}$$

Cubic B-spline function:

$$W(d) = \frac{\mathrm{G}}{\mathrm{h}^{\lambda}} \begin{cases} 1 - 1.5d^2 + 0.75d^3 & 0 \le d < 1 \\ (2-d)^3/4 & 1 \le d \le 2 \\ 0 & 2 < d \end{cases} \tag{6.6}$$

Quartic spline function:

$$W(d) = \frac{\mathrm{G}}{\mathrm{h}^{\lambda}} \begin{cases} 1 - \frac{3}{2}d^2 + d^3 - \frac{3}{16}d^4 & 0 \le d \le 2 \\ 0 & 2 < d \end{cases} \tag{6.7}$$

The revised Gauss function:

$$W(d) = \frac{G}{\left(h\sqrt{\pi}\right)^{\lambda}} \begin{cases} \left(e^{-d^2} - e^{-4}\right) & 0 \le \mathrm{d} \le 2 \\ 0 & d > 2 \end{cases} \tag{6.8}$$

The super Gauss function:

$$W(d) = \frac{G}{\left(h\sqrt{\pi}\right)^{\lambda}} \left(\frac{5}{2} - d^2\right) e^{-d^2} \tag{6.9}$$

Here $d = |\mathbf{x} - \boldsymbol{\xi}|/h$, λ equals the dimensionality of the space, G is the normalizing constant determined by the condition that the integral of the kernel function over the domain equals 1.0. For $\lambda = 1$, G equals, respectively, 1, 0.75,2/3, 5/8, and 1.04823 for the linear, the quadratic, the cubic B-spline, the Quartic spline, and the revised Gauss functions. In the MSPH and the SSPH methods, the value of G is not important as it is in the conventional SPH method since in Eqs. (2.10) and (3.1) it cancels out on both sides.

We note that the value of the super Gauss kernel function is negative at points where d^2 is greater than 5/2. As is well known, the kernel function determines the contribution of deformations of a particle to that of its neighbors. Thus, the kernel function should vanish at a particle if it does not interact with its neighbors. Accordingly, we modify the super

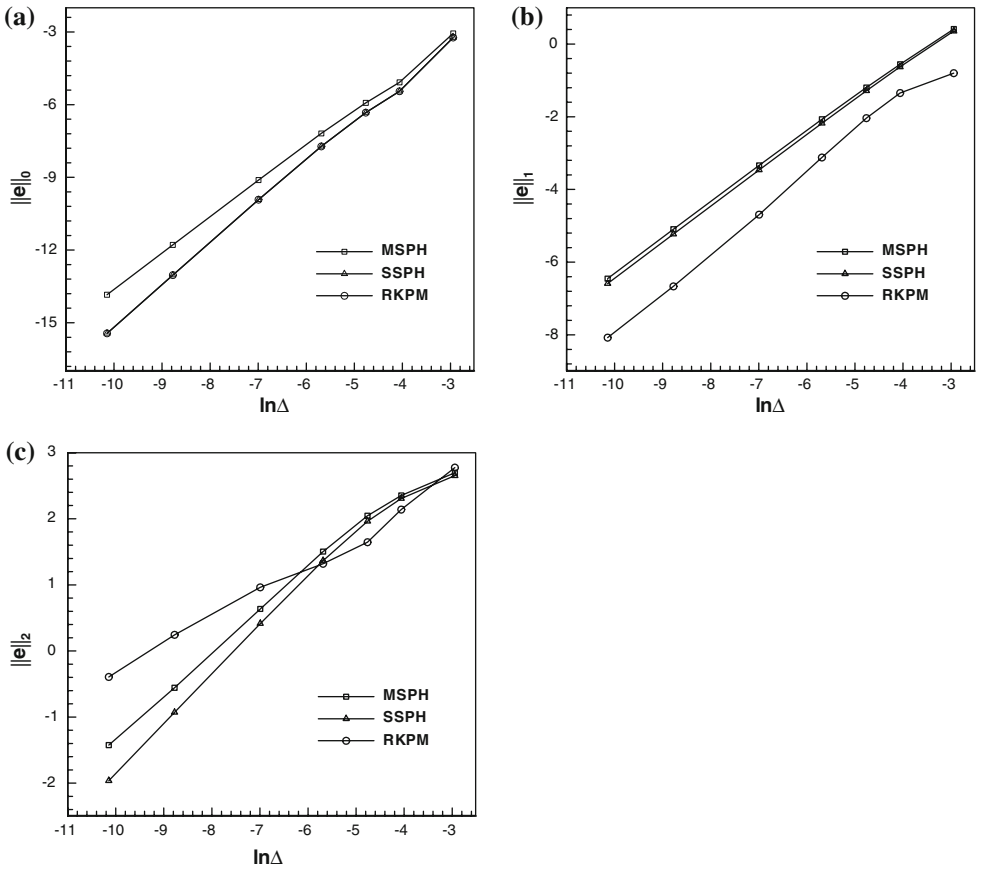

Fig. 4 Variation with different number of non-uniformly spaced particles of the (**a**) L^2 norm; (**b**) H^1 norm; and (**c**) H^2 norm of the function computed with the MSPH and the SSPH methods, and with the RKPM

Gauss kernel function to

$$W(d) = \frac{G}{\left(h\sqrt{\pi}\right)^{\lambda}} \begin{cases} \left(4 - d^2\right) e^{-d^2} & 0 \le \mathrm{d} \le 2 \\ 0 & \mathrm{d} > 2 \end{cases} \tag{6.10}$$

set $G = 2/7$ for $\lambda = 1$, and call it the revised super Gauss function. With this modification, it vanishes for $d \ge 2$ thereby ensuring that only particles that lie in the compact support of particle i influence its deformations.

For a 1D problem, Fig. 5 exhibits plots of the six kernel functions. Note that they take different values at the origin because of the normalization condition that the integral of a kernel function over its compact support equals one. Also, these kernel functions have different compact property. The cubic B-spline function has the most compact property, the revised super Gauss the next and the Quartic the third. We examine below whether the compact property of the kernel function has any influence on the accuracy of results, or the error norms.

We use the six kernel functions in the SSPH method to approximate the function $f(x) = e^{-x^2}$ and its first derivative with 20 uniformly spaced particles placed on the domain [0, 1]. Unless otherwise specified, we take the smoothing length $h = 1.2\Delta$.

The L^2 and the H^1 error norms of kernel estimates of the function f and of its first derivative f_x computed with the six

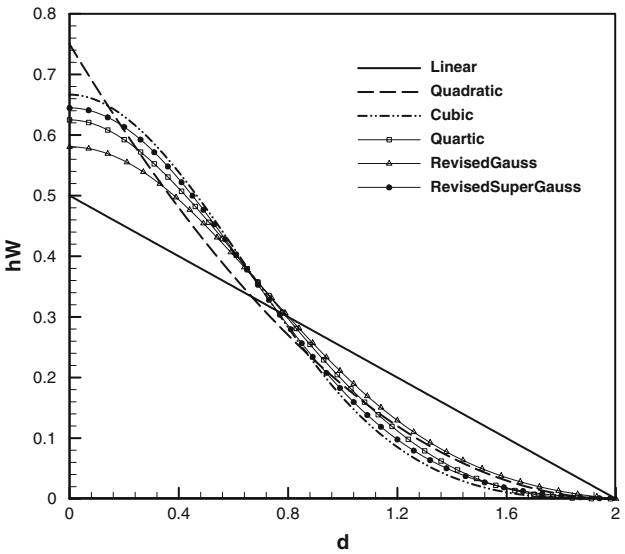

Fig. 5 For a one-dimensional problem plots of the six kernel functions

kernel functions are given in Table 3. The number in parentheses besides the error norm denotes the ranking of the error norm with 1 for the smallest, and 6 for the largest. The error norms are of the same order of magnitude for the six kernel functions. It is evident that the cubic kernel function gives

Table 3 Error norms for the six kernel functions computed with $h = 1.2\Delta$

	Linear	Quadratic	Cubic	Quartic	Revised Gauss	Revised super Gauss
$\|e\|_0$ /(E-6)	6.84 (6)	3.01 (4)	1.60 (1)	2.43 (2)	4.30 (5)	2.63 (3)
$\|e\|_1$ /(E-3)	3.12 (6)	2.12 (4)	1.56 (1)	1.70 (2)	2.19 (5)	1.80 (3)

the smallest error norm, which agrees with its most compact property. But the quartic function gives smaller values of the L^2 and the H^1 error norms than the revised super Gauss function which is opposite to the order of their compact property. We note that the quadratic and the linear kernel functions give reasonably accurate results, the quadratic function gives smaller value of the error norm than the revised Gauss function, and the linear and the quadratic kernel functions cannot be employed in the MSPH method and the RKPM since their first and second order derivatives, respectively, are constants.

For this 1D-problem, matrices **P** and **Q** defined in Eqs. (2.4) and (2.3) are given by

$$\mathbf{P} = \left\{1, \xi - x^{(i)}, \left(\xi - x^{(i)}\right)^2\right\}, \ \mathbf{Q} = \left\{f_i, f_{xi}, \frac{1}{2} f_{xxi}\right\}^T. \tag{6.11}$$

Because each kernel function is even and particles are uniformly spaced, we have

$$K_{12} = K_{21} = 0, K_{23} = K_{32} = 0, \tag{6.12}$$

at an inner particle where the matrix **K** is defined in Eq. (3.3). When the particle i has only four other particles, $i-2$, $i-1$, $i+1$ and $i+2$, in the compact support of its kernel function, we obtain from Eq. (3.6) the following expressions for the kernel estimate and the first derivative of the function f:

$$\begin{aligned} f_i &= (f_i) + \frac{\frac{W_{i,i+2}}{W_{i,i}}}{1 + 16\frac{W_{i,i+2}}{W_{i,i+1}} + 18\frac{W_{i,i+2}}{W_{i,i}}} \\ &\quad \times \left[12(f_{i+1} + f_{i-1}) - 3(f_{i+2} + f_{i-2}) - 18 f_i\right] \\ &\equiv (f_i) + c_1 \left[12(f_{i+1} + f_{i-1}) - 3(f_{i+2} + f_{i-2}) - 18 f_i\right] \end{aligned} \tag{6.13}$$

$$\begin{aligned} f_{xi} &= \frac{f_{i+1} - f_{i-1}}{2\Delta} \\ &\quad + \frac{\frac{W_{i,i+2}}{W_{i,i+1}}}{\frac{W_{i,i+2}}{W_{i,i+1}} + \frac{1}{4}} \left(\frac{f_{i+2} - f_{i-2}}{4\Delta} - \frac{f_{i+1} - f_{i-1}}{2\Delta}\right) \\ &\equiv \frac{f_{i+1} - f_{i-1}}{2\Delta} + c_2 \left(\frac{f_{i+2} - f_{i-2}}{4\Delta} - \frac{f_{i+1} - f_{i-1}}{2\Delta}\right) \end{aligned} \tag{6.14}$$

Here (f_i) stands for the value of the function f at $x^{(i)}$, and we have used the fact that the kernel function is even, i.e., $W_{i,i-1} = W_{i,i+1}$ and $W_{i,i-2} = W_{i,i+2}$. Equation (6.13) implies that when c_1 is zero the SSPH method reconstructs the function. For nonzero values of c_1 the difference between

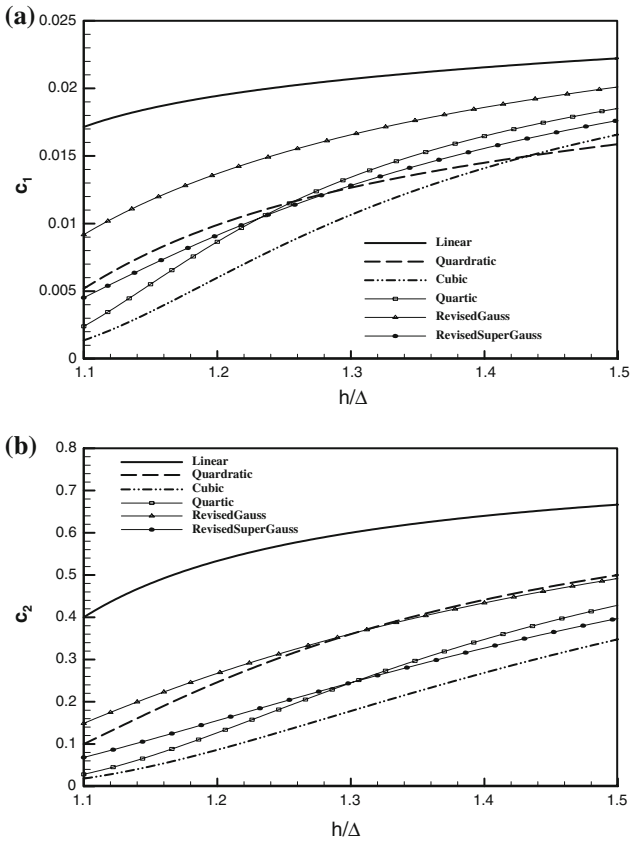

Fig. 6 For the six kernel functions, variations of (**a**) c_1; and (**b**) c_2 with the smoothing length, h

the value of the function and its kernel estimate is proportional to c_1. Also, the difference between the kernel estimates of f_x and its value computed by the central difference method is proportional to c_2.

Values of c_1 and c_2 for the six kernel functions and the smoothing length h varying from 1.1 Δ to 1.5 Δ are exhibited in Fig. 6. These values of h ensure that an inner particle i has four other particles in the compact support of its kernel function. For $h = 1.2\Delta$, the ranking of values of c_1 and c_2 for the six kernel functions is the same as that of the error norms in Table 3. From Fig. 6, we find that with the increase in the smoothing length, the order of coefficients for the six kernel functions will vary. For example, values of c_1 for the quartic and the revised super Gauss functions will change their order around $h = 1.23\Delta$. We have computed another case when the initial smoothing length is 1.4Δ and list the error norms in Table 4. By comparing results in Table 4 and Fig. 6 we conclude that the two rankings match very well.

Table 4 Error norms for the six kernel functions computed with $h = 1.4\Delta$

	Linear	Quadratic	Cubic	Quartic	Revised Gauss	Revised super Gauss
$\|e\|_0$ /(E-6)	7.82 (6)	4.86 (2)	4.44 (1)	5.43 (4)	6.36 (5)	5.06 (3)
$\|e\|_1$ /(E-3)	3.50 (6)	2.80 (5)	2.20 (1)	2.47 (3)	2.78 (4)	2.40 (2)

When the compact support of the kernel function for an inner particle i contains only three particles, that is, $W_{i,i+2} = 0$, coefficients c_1 and c_2 become zero, and Eqs. (6.13) and (6.14) simplify to

$$f_i = (f_i) \tag{6.15}$$

$$f_{xi} = \frac{f_{i+1} - f_{i-1}}{2\Delta} \tag{6.16}$$

Thus for particles inside the domain the SSPH method exactly reconstructs the original function, and the kernel estimate of the first derivative of the function equals the value of the first derivative given by the central-difference method.

We now investigate if the performance of the revised super Gauss kernel function can be improved by increasing the coefficient a in the following equation.

$$W(d) = \frac{G}{\left(h\sqrt{\pi}\right)^{\lambda}}\left(4 - d^2\right)e^{-\mathrm{a}d^2}. \tag{6.17}$$

For a =1.0, 1.2, 1.4 and 1.6, Fig. 7 evinces variations of c_1 and c_2 with the smoothing length. It is evident that values of c_1 and c_2 decrease with an increase in the values of a. When the value of a is increased from 1.0 to 1.2, c_1 and c_2 for the super Gauss function are smaller than those for the quartic function for most values of the smoothing length. For most values of the smoothing length in the range $[1.1\Delta, 1.5\Delta]$, and $a = 1.4$, the cubic function has larger values of c_1 and c_2 than the revised super Gauss function. For $a = 1.6$, both c_1 and c_2 for the revised super Gauss function have the least values for all h in the range $[1.1\Delta, 1.5\Delta]$. Thus the super Gauss function with $a = 1.6$ is expected to give smallest values of error norms, which is confirmed by their values listed in Table 5. The error norms follow the ranking predicted by values of coefficients c_1 and c_2. Even though values of coefficients c_1 and c_2 continue to decrease with an increase in the value of the parameter a, one can not take a to be very large since the effect of enough particles must be included to ensure accuracy of results. We propose that the revised super Gauss function with $a = 1.6$ be used as a kernel function.

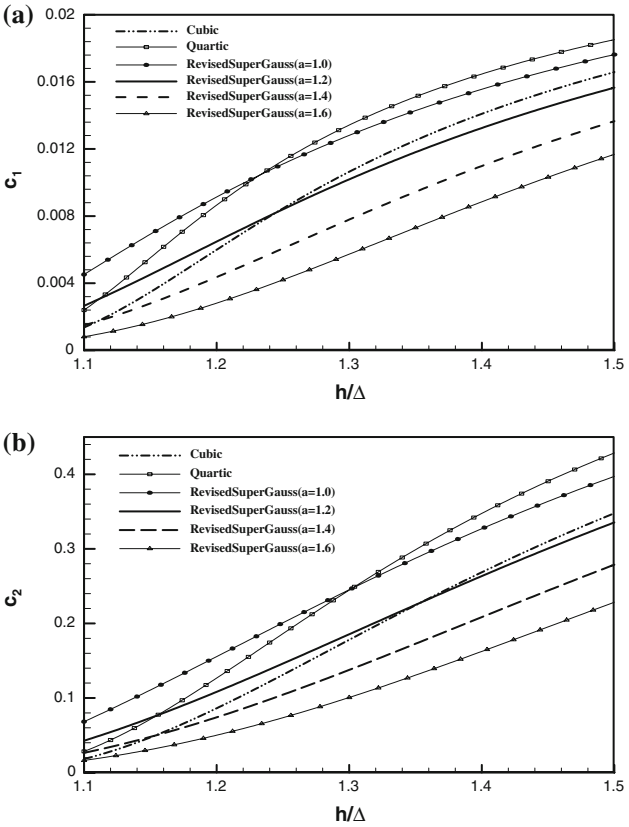

Fig. 7 For a = 1.0, 1.2, 1.4 and 1.6, variations of (**a**) c_1; (**b**) c_2 with the smoothing length h for the revised Super Gauss kernel function. Values of c_1 and c_2 for the cubic and the quartic kernel functions are also plotted for comparison

For two different values of the smoothing length $h = 1.2\Delta$ and $h = 1.4\Delta$, we have plotted in Fig. 8 the variation with the smallest distance between adjacent two particles of the H^1

Table 5 For two values of the smoothing length, error norms for the quartic and the cubic kernel functions, and the revised super Gauss kernel function with a= 1.0, 1.2, 1.4 and 1.6

Numbers in parentheses give ranking of error norms for these kernel functions

		Cubic	Quartic	Revised super Gauss			
				a = 1.0	a = 1.2	a = 1.4	a = 1.6
$h = 1.2\Delta$	$\|e\|_0$ /(E − 6)	1.60 (3)	2.43 (5)	2.63 (6)	1.77 (4)	1.14 (2)	0.71 (1)
	$\|e\|_1$ /(E − 3)	1.56 (3)	1.70 (5)	1.80 (6)	1.64 (4)	1.52 (2)	1.44 (1)
$h = 1.4\Delta$	$\|e\|_0$ /(E − 6)	4.44 (4)	5.43 (6)	5.06 (5)	4.14 (3)	3.30 (2)	2.55 (1)
	$\|e\|_1$ /(E − 3)	2.20 (4)	2.47 (6)	2.40 (5)	2.18 (3)	1.99 (2)	1.83 (1)

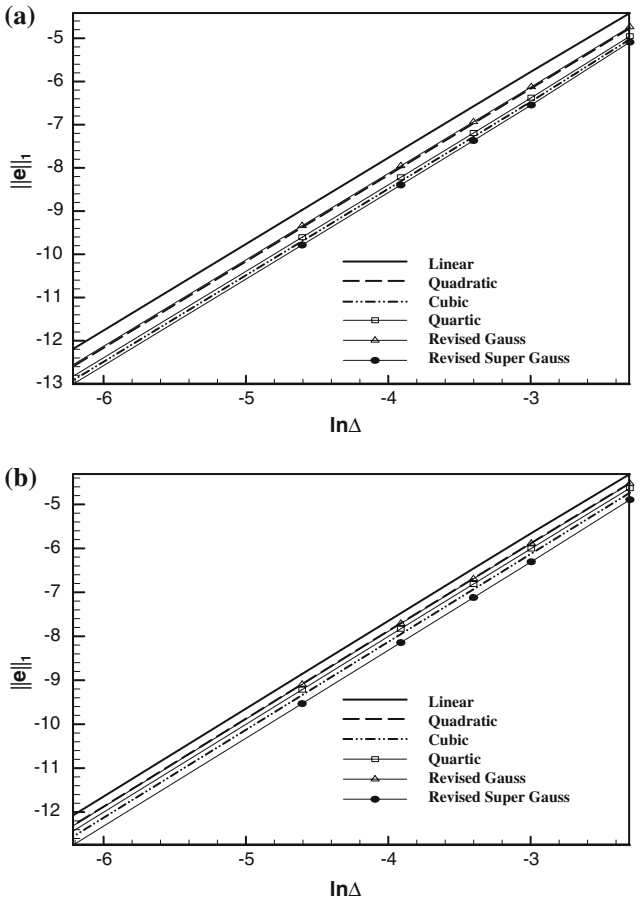

Fig. 8 For **a** $h = 1.2\Delta$ and **b** $h = 1.4\Delta$, H^1 error norms in kernel estimates computed with different kernel functions versus the smallest distance between adjacent particles

error norms of the function computed by the six kernel functions, namely, the linear, the quadratic, the cubic B-spline, the quartic, the revised Gauss, and the revised super Gauss with a = 1.6. Slopes of these curves are listed in Table 6. It can be seen that the convergence rates are not affected by the choice of the kernel function. A larger smoothing length will give smaller convergence rate.

6.3 Stress concentration in a plate

We use the SSPH method to analyze stress concentration near a circular hole in a semi-infinite isotropic and homogeneous linear elastic plate deformed statically by equal and opposite axial tractions at its two opposite edges. As shown in Fig. 9, the plate with a central hole of radius b is subjected to a constant axial tensile traction, σ_0, on the left and the right edges that are at infinity. In cylindrical coordinates (r, θ) with the origin at the center of the hole, the analytic solution [32] for the stress field $\boldsymbol{\sigma}$ and the displacement field $\mathbf{u}$ is

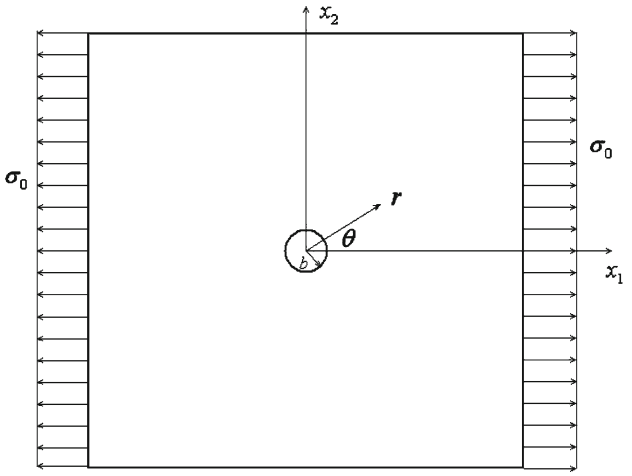

Fig. 9 Schematic sketch of a plate with a central hole loaded in tension

$$
\begin{aligned}
\sigma_{rr} &= \frac{\sigma_0}{2}\left(1-\frac{b^2}{r^2}\right)+\frac{\sigma_0}{2}\left(1+3\frac{b^4}{r^4}-4\frac{b^2}{r^2}\right)\cos 2\theta,\\
\sigma_{\theta\theta} &= \frac{\sigma_0}{2}\left(1+\frac{b^2}{r^2}\right)-\frac{\sigma_0}{2}\left(1+3\frac{b^4}{r^4}\right)\cos 2\theta,\\
\sigma_{r\theta} &= -\frac{\sigma_0}{2}\left(1-3\frac{b^4}{r^4}+2\frac{b^2}{r^2}\right)\sin 2\theta,\\
u_1 &= \frac{1+\overline{\nu}}{\overline{E}}\sigma_0\left(\frac{1}{1+\overline{\nu}}r\cos\theta+\frac{2}{1+\overline{\nu}}\frac{b^2}{r}\cos\theta\right.\\
&\quad \left.+\frac{1}{2}\frac{b^2}{r}\cos 3\theta-\frac{1}{2}\frac{b^4}{r^3}\cos 3\theta\right),\\
u_2 &= \frac{1+\overline{\nu}}{\overline{E}}\sigma_0\left(\frac{-\overline{\nu}}{1+\overline{\nu}}r\sin\theta-\frac{1-\overline{\nu}}{1+\overline{\nu}}\frac{b^2}{r}\sin\theta\right.\\
&\quad \left.+\frac{1}{2}\frac{b^2}{r}\sin 3\theta-\frac{1}{2}\frac{b^4}{r^3}\sin 3\theta\right),
\end{aligned}
\tag{6.18}
$$

where $\overline{E} = \frac{E}{1-\nu^2}$, $\overline{\nu} = \frac{\nu}{1-\nu}$, E = Young's modulus, ν = Poisson's ratio for the material of the body, and u_1 and u_2 are components, respectively, of the displacement vector $\mathbf{u}$ along the horizontal and the vertical directions.

Due to symmetry of the problem about the horizontal and the vertical centroidal axes, we analyze deformations of a quarter of the finite domain shown in Fig. 10, and assume that a plane strain state of deformation prevails in the plate. Boundary conditions in rectangular Cartesian coordinates are listed below:

$u_1 = 0, \quad t_2 = 0$	on boundary 1
$t_1 = 0, \quad t_2 = 0$	on boundary 2
$t_1 = 0, \quad u_2 = 0$	on boundary 3
$t_1 = \bar{t}_1, \quad t_2 = \bar{t}_2$	on boundaries 4 and 5

Since boundary surfaces 4 and 5 are not taken to be far away from the circular hole, we apply tractions on them with $\bar{t}_1$ and $\bar{t}_2$ determined from $\bar{t}_1 = \sigma_{11}n_1 + \sigma_{12}n_2$, $\bar{t}_2 = \sigma_{21}n_1 +$

Table 6 The convergence rate of error norms for the six kernel functions with smoothing length $h = 1.2\Delta$ and $h = 1.4\Delta$

	Linear	Quadratic	Cubic	Quartic	Revised Gauss	Revised super Gauss
$h = 1.2\Delta$	1.9902	2.0006	2.0140	2.0096	1.9993	2.0189
$h = 1.4\Delta$	1.9882	1.9926	1.9993	1.9956	1.9927	2.0064

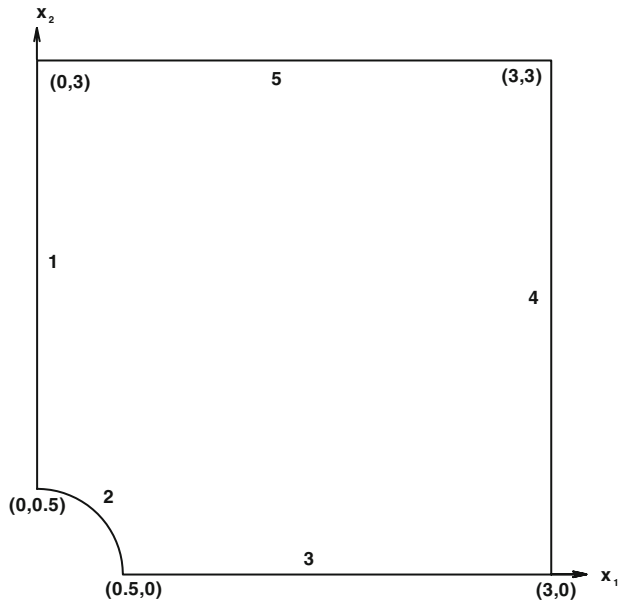

Fig. 10 The plate used in the simulation

$\sigma_{22}n_2$ where n is a unit outward normal to the boundary, and t is the traction vector, and values of σ_{11}, σ_{22} and σ_{12} are found from the analytical solution (6.18) by using tensor transformation rules; e.g. see [33]. Plate's deformations are governed by

$$\sigma_{ij,j} + g_i = 0 \text{ in } \Omega, \quad i = 1, 2, \tag{6.19}$$

$$\sigma_{ij} = \hat{\lambda}\varepsilon_{kk}\delta_{ij} + 2\hat{\mu}\varepsilon_{ij}, \tag{6.20}$$

$$\varepsilon_{ij} = \frac{1}{2}\left(\frac{\partial u_i}{\partial x_j} + \frac{\partial u_j}{\partial x_i}\right), \tag{6.21}$$

where a repeated index implies summation over the range of the index, $\mathbf{g}$ is the body force vector which is zero in our work, $\boldsymbol{\varepsilon}$ is the strain tensor, $\hat{\lambda} = \frac{E\nu}{(1+\nu)(1-2\nu)}$ and $\hat{\mu} = \frac{E}{2(1+\nu)}$ are the Lame constants. Here E is Young's modulus and ν the Poisson ratio. Substitution from Eqs. (6.20) and (6.21) into Eq. (6.19) gives

$$\begin{aligned}
&\left(\hat{\lambda} + 2\hat{\mu}\right)\frac{\partial^2 u_1}{\partial x_1^2} + \hat{\mu}\frac{\partial^2 u_1}{\partial x_2^2} + \left(\hat{\lambda} + \hat{\mu}\right)\frac{\partial^2 u_2}{\partial x_1 \partial x_2} = 0 \\
&\left(\hat{\lambda} + \hat{\mu}\right)\frac{\partial^2 u_1}{\partial x_1 \partial x_2} + \hat{\mu}\frac{\partial^2 u_2}{\partial x_1^2} + \left(\hat{\lambda} + 2\hat{\mu}\right)\frac{\partial^2 u_2}{\partial x_2^2} = 0
\end{aligned} \tag{6.22}$$

for the unknown components u_1 and u_2 of the displacement vector. By writing Eq. (2.15) of the MSPH method or Eq. (3.6) of the SSPH method as

$$\mathbf{Q} = \mathbf{K}^{-1}\mathbf{T} = \left(\mathbf{K}^{-1}\mathbf{B}\right)\mathbf{F}, \tag{6.23}$$

where

$$\begin{aligned}
B_{IJ} &= M_I^J m_J/\rho_J \qquad \text{for the MSPH method,} \\
B_{IJ} &= WP_I m_J/\rho_J \qquad \text{for the SSPH method,} \\
\mathbf{F} &= \{f_1, f_2, \cdots, f_{N_{\text{total}}}\}^T,
\end{aligned}$$

it can be seen that derivatives of u_1 and u_2 can be expressed in terms of values of u_1 and u_2 at particles in the domain. We thus arrive at $2N_{\text{total}}$ (N_{total} equals the total number of particles) simultaneous linear algebraic equations for values of u_1 and u_2 at all particles. For boundary particles, boundary conditions should be satisfied. For a particle on boundary1, the two Eqs. (6.22) for the particle are replaced by the boundary conditions

$$\begin{aligned}
u_1 &= 0 \\
t_2 &= 0
\end{aligned} \tag{6.24}$$

where $t_2 = \sigma_{21}n_1 + \sigma_{22}n_2$. Substitution from Eq. (6.20) into Eq. (6.24) gives

$$\begin{aligned}
&u_1 = 0 \\
&\hat{\mu}\left(\frac{\partial u_1}{\partial x_2} + \frac{\partial u_2}{\partial x_1}\right)n_1 + \left[\hat{\lambda}\frac{\partial u_1}{\partial x_1} + \left(\hat{\lambda} + 2\hat{\mu}\right)\frac{\partial u_2}{\partial x_2}\right]n_2 = 0
\end{aligned} \tag{6.25}$$

Similarly, equations for all boundary particles are modified. We then assemble equations for all particles and solve them simultaneously for displacements.

Figure 11 depicts the placement of 188 particles in the domain of study with 11 particles on the quarter of the circular hole. The distribution of particles gets coarser with the distance from the circular hole. Results are computed with the revised super Gauss kernel function (6.17) with $a = 1.6, \lambda = 2$, and the smoothing length $h_i = 1.5\Delta_i$ where Δ_i is the smallest distance between particle i and other particles in its compact support. Values assigned to material parameters of the plate and the tensile traction are

$$E = 1, \quad \nu = 0.25, \quad \sigma_0 = 1.$$

Along the x_2-axis, the analytical solution gives

$$\begin{aligned}
&u_1|_{\theta=\pi/2} = 0, \quad u_2|_{\theta=\pi/2} \\
&= \frac{1+\overline{\nu}}{\overline{E}}\sigma_0\left(\frac{-\overline{\nu}}{1+\overline{\nu}}x_2 - \frac{1-\overline{\nu}}{1+\overline{\nu}}\frac{b^2}{x_2} - \frac{1}{2}\frac{b^2}{x_2} + \frac{1}{2}\frac{b^4}{x_2^3}\right).
\end{aligned}$$

Values of u_2 computed with the SSPH and the MSPH basis functions are compared with those from the analytical solution in Fig. 12. It is clear that the displacement given by the SSPH method is closer to the analytic solution than that obtained with the MSPH method. The error norm defined as

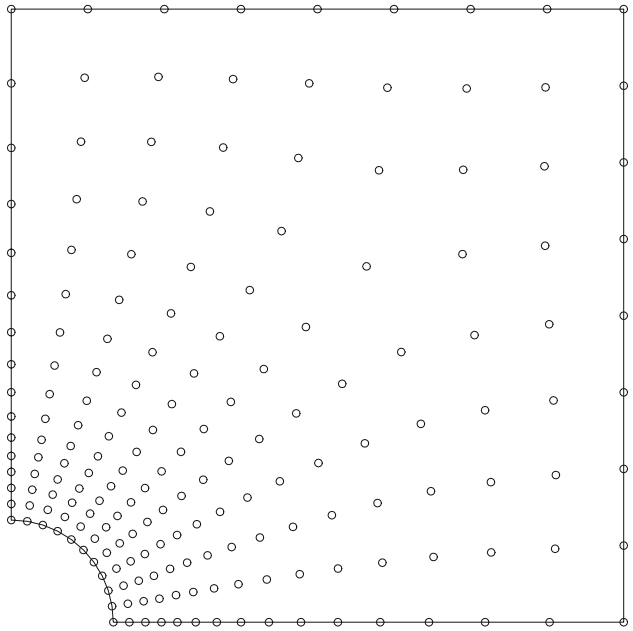

Fig. 11 Locations of 188 particles in the domain studied

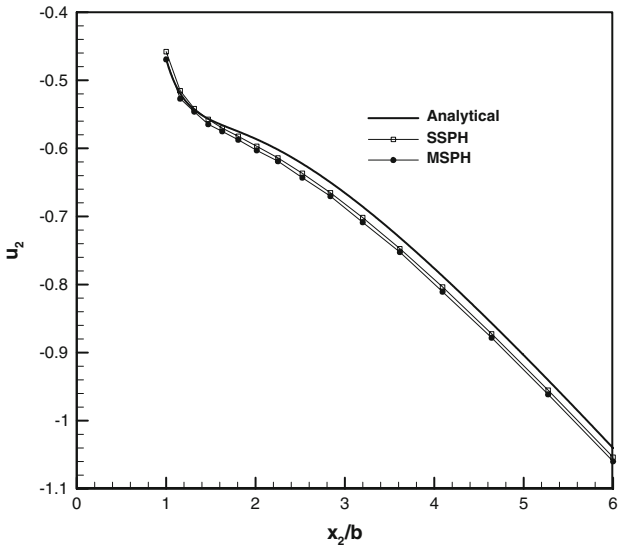

Fig. 12 Comparison of the displacement u_2 along the x_2 axis in a plate with a circular hole computed by the SSPH and the MSPH methods with that obtained from the analytical solution (188 particles)

$\sqrt{\int \left(u_2^{\text{compute}} - u_2^{\text{analytical}}\right)^2 dx_2}$ equals 0.0216 and 0.0304 for the SSPH and the MSPH methods respectively. The CPU time equals 0.16 s for both the MSPH and the SSPH methods. Although the matrix $\boldsymbol{K}$ is symmetric for the SSPH method, which can reduce the storage requirement, we do not take advantage of this symmetry and use the same algorithm as for the MSPH method to solve the system of linear algebraic equations. Thus the CPU time is the same for the two methods. Figure 13 exhibits the placement of 686 particles

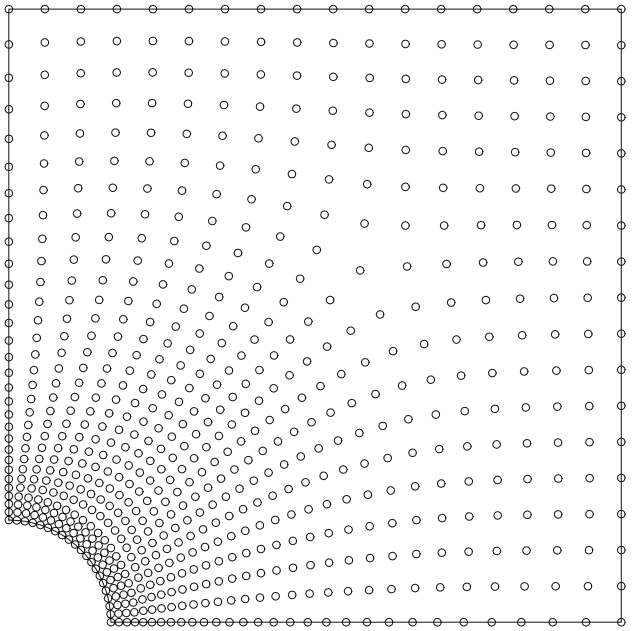

Fig. 13 Placement of 686 particles in the domain with 21 particles on quarter of the circle

with 21 particles on the quarter of the circle, and Fig. 14 compares the displacement u_2 computed with this placement of nodes with the analytical solution of the problem. The CPU time increases to about 9 s since the number of equations is increased from 376 to 1,372 and inversion of the 1372×1372 matrix takes more time than that required to invert the 376×376 matrix. We can decrease the CPU time by optimizing the algorithm for solving a system of sparse linear algebraic equations as is done in the FEM, but this is not the focus of our work. The error norms of 0.0044 and 0.0050 for displacements computed with the SSPH and the MSPH methods, respectively, indicate that the solution is significantly improved by increasing the number of particles. The corresponding values of the non-dimensional stress σ_{11}/σ_0 along the x_2-axis, exhibited in Fig. 15, reveal that the three sets of values are very close to each other. Both the SSPH and the MSPH methods accurately predict the stress concentration of 3.0.

We note that here a strong form of differential equations (6.19) is solved, and the technique can be viewed as the collocation method employing the SSPH basis functions.

6.4 Elastodynamic problem

In the elastostatic problem studied above, it is shown that the SSPH method gives better results than the MSPH method. We now only use the SSPH method to solve a linear elastodynamic problem. Whereas a 3D problem has been formulated, the solution is given only for a 1D problem, namely, wave propagation in a bar.

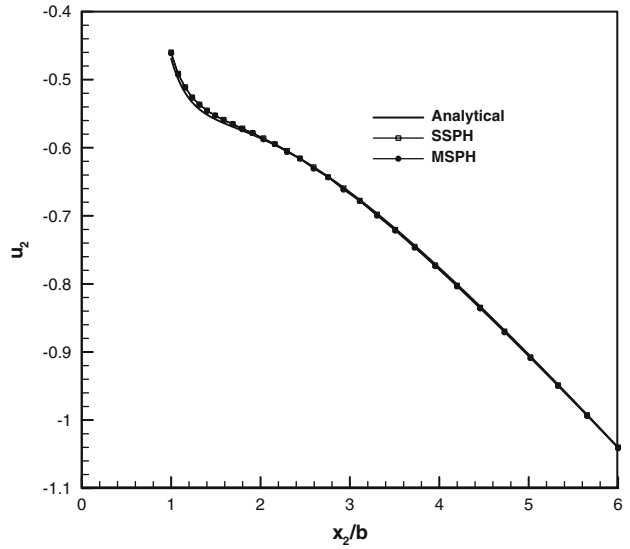

Fig. 14 Comparison of the displacement u_2 along the x_2 axis in a plate with a circular hole computed by the SSPH and the MSPH methods with that obtained from the analytical solution (686 particles)

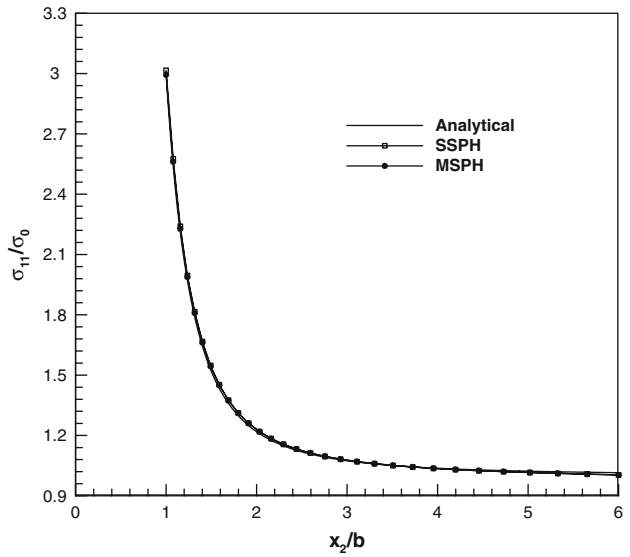

Fig. 15 Comparison of the non-dimensional stress σ_{11}/σ_0 along the x_2 axis in a plate with a circular hole computed by the SSPH and the MSPH methods with that obtained from the analytical solution (686 particles)

In the absence of body force, deformations of a body are governed by the following equation expressing the balance of linear momentum:

$$\rho \frac{d^2 u_i}{dt^2} = \sigma_{ij,j} \tag{6.26}$$

where ρ is the mass density. Substituting into Eq. (6.26) for stresses in terms of strains from Hooke's law (6.20) and for strains in terms of displacements from Eq. (6.21), we get

$$\rho \begin{Bmatrix} \ddot{u}_1 \\ \ddot{u}_2 \\ \ddot{u}_3 \end{Bmatrix} = \begin{bmatrix} \left(\hat{\lambda}+\hat{\mu}\right)\frac{\partial^2}{\partial x_1^2}+\hat{\mu}\nabla^2 & \left(\hat{\lambda}+\hat{\mu}\right)\frac{\partial^2}{\partial x_1 \partial x_2} & \left(\hat{\lambda}+\hat{\mu}\right)\frac{\partial^2}{\partial x_1 \partial x_3} \\ \left(\hat{\lambda}+\hat{\mu}\right)\frac{\partial^2}{\partial x_1 \partial x_2} & \left(\hat{\lambda}+\hat{\mu}\right)\frac{\partial^2}{\partial x_2^2}+\hat{\mu}\nabla^2 & \left(\hat{\lambda}+\hat{\mu}\right)\frac{\partial^2}{\partial x_2 \partial x_3} \\ \left(\hat{\lambda}+\hat{\mu}\right)\frac{\partial^2}{\partial x_1 \partial x_3} & \left(\hat{\lambda}+\hat{\mu}\right)\frac{\partial^2}{\partial x_2 \partial x_3} & \left(\hat{\lambda}+\hat{\mu}\right)\frac{\partial^2}{\partial x_3^2}+\hat{\mu}\nabla^2 \end{bmatrix} \begin{Bmatrix} u_1 \\ u_2 \\ u_3 \end{Bmatrix} \tag{6.27}$$

where $\nabla^2 = \frac{\partial^2}{\partial x_1^2} + \frac{\partial^2}{\partial x_2^2} + \frac{\partial^2}{\partial x_3^2}$ is the Laplace operator, and a superimposed dot indicates time derivative.

The boundary conditions are

$$u_i = \bar{u}_i \text{ on } \Gamma_u, \tag{6.28}$$

$$\sigma_{ij} n_j = \bar{t}_i \text{ on } \Gamma_t. \tag{6.29}$$

The natural boundary condition (6.29) can be written in terms of displacements as

$$\begin{aligned} &\left[\left(\hat{\lambda}+2\hat{\mu}\right)\frac{\partial u_1}{\partial x_1}+\hat{\lambda}\frac{\partial u_2}{\partial x_2}+\hat{\lambda}\frac{\partial u_3}{\partial x_3}\right] n_1 + \hat{\mu}\left(\frac{\partial u_1}{\partial x_2}+\frac{\partial u_2}{\partial x_1}\right) n_2 + \hat{\mu}\left(\frac{\partial u_1}{\partial x_3}+\frac{\partial u_3}{\partial x_1}\right) n_3 = \bar{t}_1 \\ &\hat{\mu}\left(\frac{\partial u_1}{\partial x_2}+\frac{\partial u_2}{\partial x_1}\right) n_1 + \left[\left(\hat{\lambda}+2\hat{\mu}\right)\frac{\partial u_1}{\partial x_1}+\hat{\lambda}\frac{\partial u_2}{\partial x_2}+\hat{\lambda}\frac{\partial u_3}{\partial x_3}\right] n_2 + \hat{\mu}\left(\frac{\partial u_2}{\partial x_3}+\frac{\partial u_3}{\partial x_2}\right) n_3 = \bar{t}_2 \\ &\hat{\mu}\left(\frac{\partial u_1}{\partial x_3}+\frac{\partial u_3}{\partial x_1}\right) n_1 + \hat{\mu}\left(\frac{\partial u_2}{\partial x_3}+\frac{\partial u_3}{\partial x_2}\right) n_2 + \left[\left(\hat{\lambda}+2\hat{\mu}\right)\frac{\partial u_1}{\partial x_1}+\hat{\lambda}\frac{\partial u_2}{\partial x_2}+\hat{\lambda}\frac{\partial u_3}{\partial x_3}\right] n_3 = \bar{t}_3 \end{aligned} \tag{6.30}$$

Equations (6.27) are integrated with respect to time by employing the explicit central difference method. For nodes on the boundary, Eqs. (6.27) are replaced by either Eq. (6.28) or Eq. (6.29). Expressions for displacement derivatives in terms of displacements of particles are derived by using the SSPH basis functions as was done for the elastostatic problem studied above.

These equations are used to study wave propagation in a linear elastic bar subjected to an impulsive load, and values assigned to the three material parameters are

$$E = 200GPa, \quad \nu = 0.3, \quad \rho = 7865\,\text{Kg/m}^3$$

We assume that a 0.1 m long linear elastic bar is subjected to an axial compressive step traction of 1 GPa magnitude and 3 μs duration at the right end, while its left end is kept traction free. The bar is discretized into 800 uniformly distributed particles. The analytical solution of the problem is plotted in

Fig. 16 with a dash-dot-dot curve, and the numerical solution computed with the SSPH method is depicted in Fig. 16 with a solid curve. It is clear that the SSPH method captures the shock wave very well except for some oscillations near the shock front which can be controlled by introducing artificial viscosity. The wave travels with a speed of 5 mm/μs. The compressive wave at the left end is reflected back as a tensile wave. The numerical results clearly show that there is no tensile instability.

The MSPH method was used in [34] to study wave propagation in a functionally graded bar with material properties varying continuously, in [35] to analyze crack propagation in a linear elastic plate; and in [36] to investigate the Taylor impact test. We anticipate that the SSPH method will give equally good results for these problems.

6.5 Comparison of SSPH and FE methods

The SSPH and the FE methods are compared in Table 7.

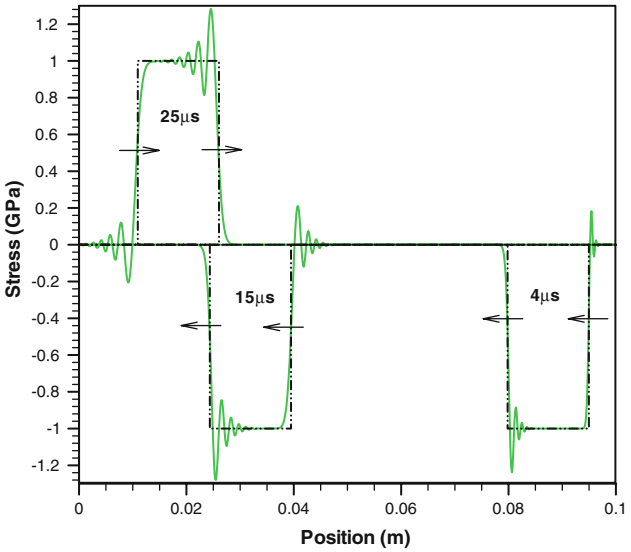

Fig. 16 Comparison of the axial stress (*solid curve*) in a bar computed by the SSPH method with that (*dash-dot curve*) obtained from the analytical solution

Table 7 Comparison of SSPH and FE methods

	SSPH	FE
Weak form	Not required	Global
Information needed about nodes	Locations only	Locations and connectivity
Subdomains	Circular/rectangular (correspond to supports of kernel functions), not necessarily disjoint	Polygonal and disjoint
Basis functions	Polynomials, require more CPU time to find them	Polynomials, easy to find
Derivatives of trial solution	Easy to evaluate	Require more CPU time to evaluate them
Integration rule	Not needed in the collocation method	Depends upon the degree of polynomials in basis functions
Mass/stiffness matrix	Asymmetric, large bandwidth that can not be determined a priori	Symmetric, banded, mass matrix positive definite, stiffness matrix positive definite after imposition of essential boundary conditions
Assembly of equations	Not required	Required
Stresses/strains	Smooth everywhere	Good at integration points
Addition of nodes/particles	Easy	Difficult
Determination of time step size	Easy	Easy
Computation of total strain energy	Difficult (requires a background mesh)	Easy
Data preparation effort	Little	Extensive
Imposition of essential boundary conditions	Easy	Easy

7 Conclusions

We have presented a symmetric smoothed particle hydrodynamics (SSPH) method that uses only locations of particles to generate basis functions. It has the following three advantages over the modified smoothed particle hydrodynamics (MSPH) method: (i) the matrix to be inverted is symmetric, (ii) a larger class of kernel functions can be used, and (iii) it yields more accurate results at least for the problems studied herein.

We have also compared kernel estimates of a function from the SSPH method with those from the reproducing kernel particle method (RKPM) and shown that these two methods give identical values of the kernel estimate of a function but different values of the kernel estimates of the first and the second derivatives of a function. For the example problem studied, the H^1 norm of the error for the RKPM is smaller than that for the SSPH method but the reverse holds for the H^2 norm of the error.

When comparing the SSPH basis functions with the moving least squares (MLS) basis functions we found that kernel estimates of derivatives of a function in the SSPH method are evaluated by solving a system of algebraic equations but in the MLS approximation they are determined by differentiating the MLS basis functions. Thus the kernel function in the MLS basis functions must be differentiable.

Numerical experiments with approximating a sine function defined on a one-dimensional domain show that the kernel estimates of the function, and its first and second derivatives computed with the SSPH method agree well with their analytical values.

We have also delineated the dependence of the L^2 error norms in the kernel estimates of the function and its first two derivatives upon the smallest distance between two adjacent particles for a uniform and a non-uniform distribution of particles.

Effects of six kernel functions on the accuracy of kernel estimates of a function, and its derivatives have been studied. The linear and the quadratic kernel functions that cannot be used in some meshless methods including the SPH and the MSPH methods, and the RKPM give good results for the SSPH method. It is found that two coefficients c_1 and c_2 whose values depend upon the rate of decay of a kernel function determine the accuracy of computed results. The ranking of the L^2 and the H^1 error norms is the same as that of values of these two coefficients for the six kernel functions. We recommend that the revised super Gauss function with the coefficient a $= 1.6$, which has the least value of the error norms be used as the kernel function. The convergence rate of the error norm for the SSPH method is the same for each one of the six kernel functions studied herein.

The displacement and the stress fields computed with the SSPH method in a rectangular elastic plate with a central hole and pulled axially on two opposite edges are found to agree well with those obtained from the analytic solution. The error norm for the solution with the SSPH method is less than that for the solution computed with the MSPH method.

The numerical solution of the one-dimensional wave propagation in a bar agrees well with the analytical solution of the problem revealing that the SSPH method captures well the shock and does not exhibit tensile instability.

Acknowledgments This work was partially supported by the ONR grant N00014-06-1-0567 to Virginia Polytechnic Institute and State University (VPI&SU) with Dr. Y. D. S. Rajapakse as the program manager. Views expressed herein are those of authors, and neither of the funding agency nor of VPI&SU.

References

1. Lucy LB (1977) A numerical approach to the testing of the fission hypothesis. Astron J 82:1013–1024
2. Chen JK, Beraun JE, Jin CJ (1999) An improvement for tensile instability in smoothed particle hydrodynamics. Comput Mech 23:279–287
3. Chen JK, Beraun JE, Jin CJ (1999) Completeness of corrective smoothed particle method for linear elastodynamics. Comput Mech 24:273–285
4. Liu WK, Jun S, Zhang YF (1995) Reproducing kernel particle methods. Int J Num Meth Fl 20:1081–1106
5. Liu WK, Jun S, Li S, Adee J, Belytschko T (1995) Reproducing kernel particle methods for structural dynamics. Int J Num Meth Eng 38:1655–1679
6. Chen JS, Pan C, Wu CT, Liu WK (1996) Reproducing kernel particle methods for large deformation analysis of non-linear structures. Comput Method Appl M 139:195–227
7. Zhang GM, Batra RC (2004) Modified smoothed particle hydrodynamics method and its application to transient problems. Comput Mech 34:137–146
8. Batra RC, Zhang GM (2004) Analysis of adiabatic shear bands in elasto-thermo- viscoplastic materials by modified smoothed-particle hydrodynamics (MSPH) method. J Comput Phys 201:172–190
9. Libersky LD, Petschek AG, Carney TC, Hipp JR, Allahdadi FA (1993) High strain Lagrangian hydrodynamics: a three-dimensional SPH code for dynamic material response. J Comput Phys 109:67–75
10. Petschek AG, Libersky LD (1993) Cylindrical smoothed particle hydrodynamics. J Comput Phys 109:76–83
11. Capuzzo-Dolcetta R, Lisio RD (2000) A criterion for the choice of the interpolation kernel in smoothed particle hydrodynamics. Appl Numer Math 34:363–371
12. Batra RC, Zhang GM (2008) SSPH basis functions for meshless methods, and comparison of solutions with strong and weak formulations. Comput Mech 41:527–545
13. Kim DW, Liu WK (2006) Maximum principle and convergence analysis for the meshfree point collocation method. SIAM J Numer Anal 44:515–539
14. Kim DW, Yoon YC, Liu WK, Belytschko T (2007) Extrinsic meshfree approximation using asymptotic expansion for interfacial discontinuity of derivative. J Comput Phys 221:370–394
15. Li SF, Liu WK (1999) Reproducing kernel hierarchical partition of unity, part I-formulation and theory. Int J Num Meth Eng 45:251–288

16. Li SF, Liu WK (1999) Reproducing kernel hierarchical partition of unity, part II-applications. Int J Num Meth Eng 45:289–317
17. Belytschko T, Krongauz Y, Dolbow J, Gerlach C (1998) On the completeness of meshfree particle methods. Int J Num Meth Eng 43:785–819
18. Gunther F, Liu WK, Diachin D, Christon MA (2000) Multi-scale mehsfree parallel computations for viscous, compressible flows. Comput Methods Appl Mech Eng 190:279–303
19. Li S, Lu H, Han W, Liu WK, Simkins DC Jr (2004) Reproducing kernel element method, Part II. Global conforming $\mathbf{I}^{\mu}/C^{n}$ hierarchy. Comput Methods Appl Mech Eng 193:953–987
20. Liu WK, Han W, Lu H, Li S, Cao J (2004) Reproducing kernel element method: Part I. Theoretical formulation. Comput Methods Appl Mech Eng 193:933–951
21. Lu H, Li S, Simkins DCJr, Liu WK, Cao J (2004) Reproducing kernel element method, Part III. Generalized enrichment and applications. Comput Methods Appl Mech Eng 193:989–1011
22. Simkins DC Jr, Li S, Lu H, Liu WK (2004) Reproducing kernel element method, Part IV. Globally compatible $C^{n}(n > 1)$ triangular hierarchy. Comput Methods Appl Mech Eng 193:1013–1034
23. Li S, Liu WK (1998) Synchronized reproducing kernel interpolant via multiple wavelet expansion. Comput Mech 21:28–47
24. Lancaster P (1969) Theory of matrices. Academic Press, New York
25. David PJ (1963) Interpolation and approximation. Dover, New York
26. Lancasater P, Salkauskas K (1981) Surface generated by moving least squares method. Math Comput 37:141–158
27. Belytschko T, Lu YY, Gu L, Tabbara M (1995) Element-free methods for static and dynamic fracture. Int J Solids Struct 32:2547–2570
28. Beissel S, Belytschko T (1996) Nodal integration of the element-free Galerkin method. Comput Method Appl M 139:49–74
29. Monaghan JJ (1992) Smoothed particle hydrodynamics. Annu Rev Astron Astr 30:543–574
30. Belytschko T, Krongauz Y, Organ D, Fleming M, Krysl P (1996) Meshless methods: an overview and recent developments. Comput Method Appl M 139:3–47
31. Gingold RA, Monaghan JJ (1982) Kernel estimates as a basis for particle methods. J Comput Phys 46:429–453
32. Li J, Zhang XB (2006) A criterion study for non-singular stress concentrations in brittle or quasi-brittle material. Eng Fract Mech 73:505–523
33. Batra RC (2005) Elements of continuum Mechanics. AIAA, Reston
34. Zhang GM, Batra RC (2007) Wave propagation in functionally graded materials by modified smoothed particle hydrodynamics (MSPH) method. J Comput Phys 222:374–390
35. Batra RC, Zhang GM (2007) Search algorithm, and simulation of elastodynamic crack propagation by modified smoothed particle hydrodynamics (MSPH) method. Comput Mech 40:531–546
36. Batra RC, Zhang GM (2008) Modified smoothed particle hydrodynamics (MSPH) methods, and their application to axisymmetric Taylor impact test. J Comput Phys 227:1962–1981